Lithos 260 (2016) 211–224

Contents lists available at ScienceDirect

Lithos

journal homepage: www.elsevier.com/locate/lithos

High-Mg adakitic rocks and their complementary cumulates formed by crystal fractionation of hydrous mafic magmas in a continental crustal magma chamber

Qiang Ma [a,b,c,*], Yi-Gang Xu [a], Jian-Ping Zheng [b], Min Sun [c], William L. Griffin [d], Ying Wei [b], Liang Ma [a], Xiaolu Yu [b]

[a] State Key Laboratory of Isotope Geochemistry, Guangzhou Institute of Geochemistry, Chinese Academy of Sciences, Guangzhou 510640, China
[b] State Key Laboratory of Geological Processes and Mineral Resources, School of Earth Sciences, China University of Geosciences, Wuhan 430074, China
[c] Department of Earth Sciences, The University of Hong Kong, Pokfulam Road, Hong Kong, China
[d] ARC CoE for Core to Crust Fluid Systems/GEMOC, Macquarie University, NSW 2109, Australia

ARTICLE INFO

Article history:
Received 15 March 2016
Accepted 31 May 2016
Available online 10 June 2016

Keywords:
Adakitic rocks
Complementary cumulates
Crystal fractionation
Hydrous magma
Deep-seated crust

ABSTRACT

Understanding how adakitic magmas form is important for understanding the formation of the continental crust. Generating such high-Sr/Y rocks by crystal fractionation of basalts/basaltic andesites in magma chambers has been proposed in a wide range of tectonic settings. However, the complementary cumulates predicted by this scenario have rarely been observed. The late Triassic (~227 Ma) Ningcheng complex from the North China Craton is composed of a websterite - (Ol—/Hbl-) pyroxenite - gabbro unit and a quartz-diorite unit. They are interpreted as the products (cumulates and derivative melts, respectively) of fractionation from hydrous mafic magmas at mid- to lower-crustal pressures (4.9 ~ 8.3 kbar). The quartz diorites are high-Mg intermediate rocks with moderate SiO_2 (57.0 ~ 62.9 wt%), high Mg# (>49) and adakitic trace element signatures, such as high Sr (≥636 ppm) and light rare earth elements (REEs), low Y (≤17 ppm) and heavy REEs (Yb ≤ 1.8 ppm), lack of obvious Eu anomalies, and high Sr/Y (≥31) and La/Yb (≥24)). These adakitic signatures reflect differentiation of hydrous mantle-derived magmas in the deep crust, leaving behind a plagioclase-free residual solid assemblage in the early stages, which is represented by the coeval websterite-pyroxenite complex. This study therefore not only demonstrates that hydrous crystal fractionation is an important mechanism to form adakitic rocks, but also presents an example of a preserved fractionating system, i.e. high-Sr/Y rocks and their complementary cumulates. A geochemical comparison is made between representative adakitic rocks formed by fractionation of hydrous magmas and Archean TTGs. It is suggested that crystal fractionation is an efficient process for making Phanerozoic high Sr/Y rocks but was not responsible for the formation of Archean granitoids.

1. Introduction

A relatively large group of intermediate to felsic igneous rocks possess many compositional features of "adakite" (Castillo, 2012; Ma et al., 2015), which commonly is proposed to be derived from partial melting of subducted oceanic basaltic crust and is mainly characterized by its high Sr/Y and La/Yb ratios (Defant and Drummond, 1990; Moyen, 2009). These adakitic rocks have attracted increasing attention because: 1) they are compositionally similar to the Archean tonalite-trondhjemite-granodiorite (TTG) suites (Martin, 1999) and therefore can improve our understanding of continental crustal evolution (Castillo, 2012; Martin et al., 2005); 2) they are associated with most porphyry-type Cu ± Mo ± Au deposits worldwide (Cooke et al., 2005; Richards and Kerrich, 2007); 3) some of them are genetically linked to partial melting of subducted oceanic slabs (Defant and Drummond, 1990; Kay, 1978) or foundered lower continental crust (Huang et al., 2008; Liu et al., 2010b), which makes them pivotal to understanding processes of crustal recycling.

Various models have been proposed to account for the origin of intermediate-felsic igneous rocks with adakitic signatures (Castillo, 2012; Martin et al., 2005), with emphasis on melting depth (Defant and Drummond, 1990; Gao et al., 2004), source inheritance (Ma et al., 2012, 2015; Qian and Hermann, 2013) and magma processes (Castillo et al., 1999; Macpherson et al., 2006). Among these models, fractional crystallization of basaltic magmas, leaving behind a plagioclase-free cumulate assemblage in the deep crust, is recognized as an important mechanism that could be responsible for subduction-related and collision-related adakitic rocks (Lu et al., 2015; Richards and Kerrich,

* Corresponding author at: State Key Laboratory of Isotope Geochemistry, Guangzhou Institute of Geochemistry, Chinese Academy of Sciences, Guangzhou 510640, China.
E-mail addresses: maqiang@gig.ac.cn, maqiang32@126.com (Q. Ma).

http://dx.doi.org/10.1016/j.lithos.2016.05.024
0024-4937/

2007). A recently statistical treatment (Chiaradia, 2015) of geochemical data on magmatic rocks from Pliocene-Quaternary arcs around the Earth also suggests that intra-crustal fractionation of mafic magmas is the main parameter controlling the development of adakitic signatures of igneous rocks. If so, there should be abundant complementary cumulates/residues of these adakitic rocks and these might play a significant role in the formation and differentiation of the continental crust (Lee, 2014; Lee et al., 2007; Müntener et al., 2001). However, such cumulate rocks have rarely been observed in nature, either because they may be located deep in the crust, and thus are inaccessible, or they may have delaminated into the mantle.

In this contribution, we present a combined field, petrologic, mineralogical and geochemical study of the Ningcheng igneous complex in the North China Craton (NCC). We demonstrate that this complex is composed of high-Sr/Y rocks and their complementary cumulates and was formed by hydrous crystal fractionation process at mid- to lower-crustal pressures. A geochemical comparison of representative differentiated adakitic rocks, modern arc magmas and Archean granitoids is further used to evaluate the role of crystal fractionation in generating high-Sr/Y rocks through geological time.

2. Geological Setting

The NCC (Fig. 1a) is one of the oldest Archean cratons in the world; it preserves ≥3.8 Ga crustal remnants both at the surface (Liu et al., 1992) and at lower-crustal levels (Zheng et al., 2004). This craton underwent a series of tectono-thermal events in late Archean and Paleoproterozoic time, and was stabilized in late Paleoproterozoic (~1.85 Ga; Zhao et al., 2001). From the late Paleoproterozoic (~1.85 Ga) to the Paleozoic (~250 Ma), it was stable without significant tectono-thermal events and was covered by a thick sequence of sediments. Multiple subduction cycles took place around the NCC in the Phanerozoic (Windley et al., 2010), including the Paleozoic southward subduction of the Paleo-Asian oceanic plate, the Triassic deep subduction of Yangtze continental crust and the Mesozoic-Cenozoic (and ongoing) subduction of the (Paleo-) Pacific plate. Meanwhile, the eastern part of this craton lost its lithospheric keel (>100 km) in the Mesozoic and Cenozoic, and represents the best known example of craton-root destruction (Carlson et al., 2005; Griffin et al., 1998; Menzies et al., 1993; Xu, 2001; Zheng et al., 2007; Zhu et al., 2012).

The Ningcheng igneous complex is located in the northern part of the NCC (Fig. 1a). This region consists of Archean to Paleoproterozoic basement rocks overlain by unmetamorphosed Mesoproterozoic to Paleozoic sediments and Mesozoic to Cenozoic sedimentary and igneous rocks. It was subjected to post-collisional extension in the early Mesozoic, intraplate contraction in the late Jurassic and crustal extension in the early Cretaceous. The Ningcheng complex intruded into the Archean basement as stocks of variable size in early Mesozoic time (Fig. 1b). The exhumation of this complex probably started in the early Cretaceous, accompanied by the development of metamorphic core complexes and granitoid magmatism.

3. Field Relationships and Petrography

The Ningcheng complex is a zoned sequence of ultramafic to felsic plutonic rocks, which consists of an ultramafic-mafic cumulate unit in the center and a quartz diorite unit in the outer part. The contact

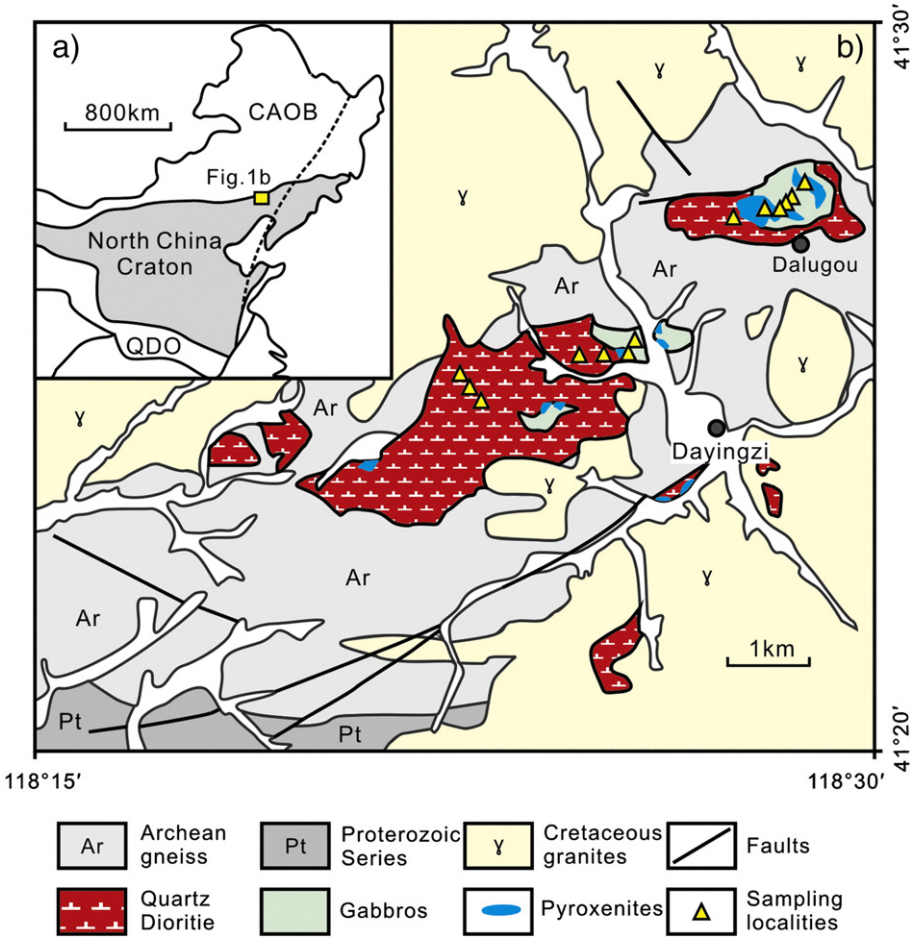

Fig. 1. Simplified geological map of Dayingzi town in the Ningcheng area (modified from Shao et al. (1999)) with inset showing location in the North China Craton.

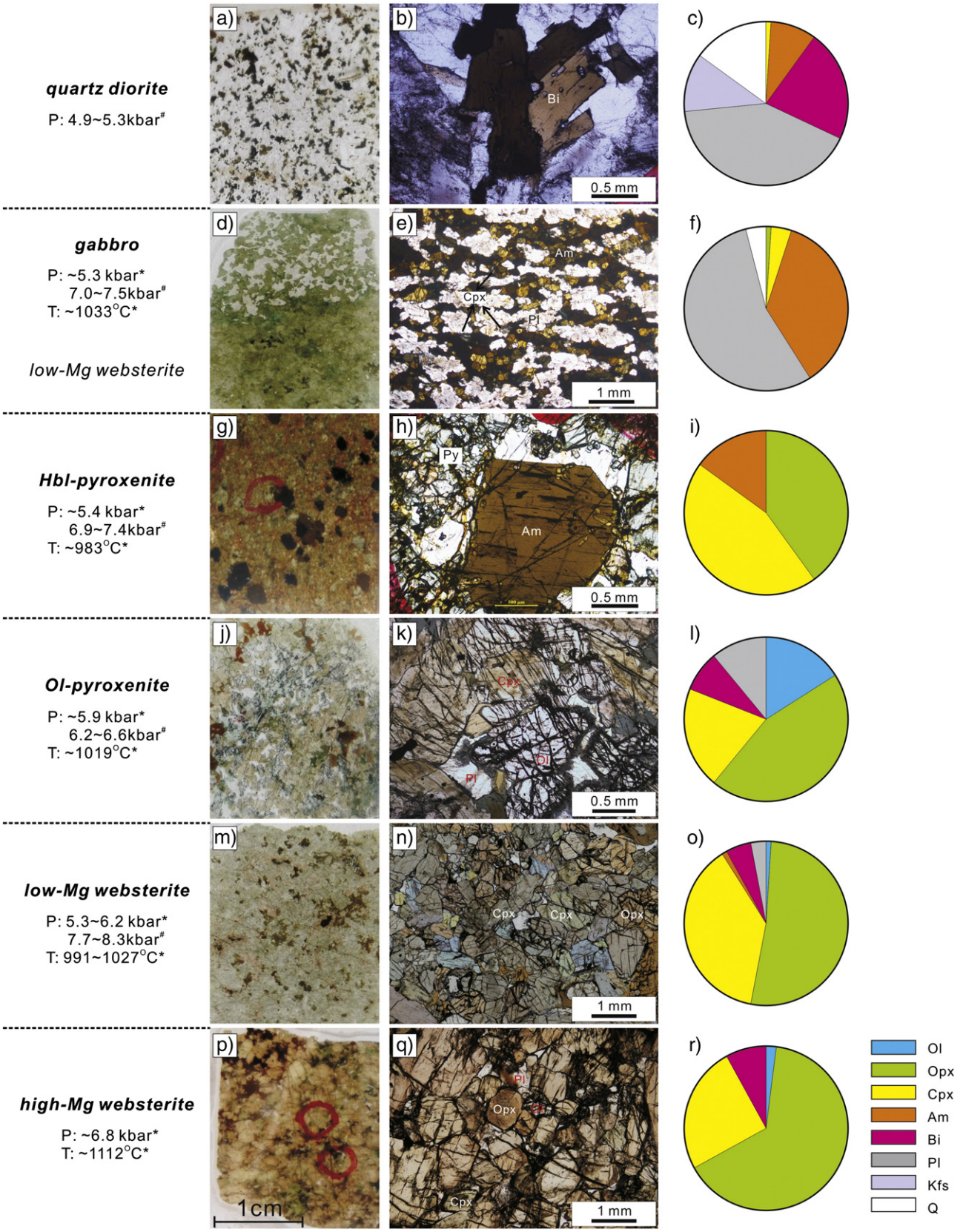

Fig. 2. Thin sections, photomicrographs (plane-polarized light) and modal compositions of representative samples of the Ningcheng complex in the North China Craton. The crystallization pressure and temperature are estimated by Al-in-hornblende barometers (marked with superscript #) and two-pyroxene thermobarometer (marked with *), and are also listed in Table 1.Mineral abbreviations: Opx, orthopyroxene; Cpx, clinopyroxene; Ol, olivine; Am, amphibole; Bi, biotite; Pl, plagioclase; Kfs, K-feldspar; Q, quartz.

between these two units is generally gradual but locally sharp, indicating that they might be coeval.

3.1. Ultramafic-mafic cumulate unit

The cumulate unit is layered and consists, from bottom to top, of high-Mg websterite (MgO > 26%), low-Mg websterite (MgO < 20%) interlayered with minor plagioclase (Pl)-bearing olivine (Ol-) pyroxenite and porphyritic hornblende (Hbl-) pyroxenite, and gabbro interlayered with minor anorthosite. Photomicrographs and modal compositions of representative samples are shown in Fig. 2.

The websterites are adcumulates containing medium to coarse grained, euhedral to subhedral cumulate pyroxene (80 ~ 95%), olivine (<5%) and magnetite (<5%) crystals and fine, anhedral interstitial plagioclase (<5%) and biotite (5 ~ 10%). Based on modal and chemical compositions, these websterites can be subdivided into a high-Mg group (MgO > 25%) with less than 25% clinopyroxene and a low-Mg group (MgO < 20%) with more than 35% clinopyroxene (Fig. 2o and 2r).

Some sub-meter to meter-scale layers of Pl-bearing Ol-pyroxenite and porphyritic Hbl-pyroxenite are observed within the low-Mg websterites. The Pl-bearing Ol-pyroxenites are also adcumulates, but contain less pyroxene (55 ~ 65%) and more plagioclase (~10%) and olivine (>15%) than the websterites. The Hbl-pyroxenites are porphyritic with phenocrysts of medium-grained (2 ~ 5 mm), euhedral hornblende (10 ~ 15%) and pyroxene (5 ~ 10%) in a groundmass of fine-grained pyroxene.

The upper part of the cumulate unit is dominated by gabbro associated with some anorthosite layers. These gabbros are composed of subparallel cumulus plagioclase (40 ~ 60%), hornblende (30 ~ 40%) and clinopyroxene (5 ~ 20%) crystals and accessory titanite, apatite and zircon.

3.2. Quartz diorite unit

The quartz diorite unit, the major lithology of the complex, is relatively homogeneous and is composed of hornblende quartz diorite and biotite quartz diorite. They are medium grained and contain 40 ~ 60% plagioclase, 20 ~ 30% biotite and hornblende, 10 ~ 20% quartz, <15% K-feldspar and <5% clinopyroxene (Fig. 2a-c). Lower-crustal granulites are found as xenoliths in the biotite quartz diorite in the western part of this unit (Shao et al., 2000).

4. Analytical Methods

4.1. Whole-rock chemistry and Sr-Nd isotopes

Major-element compositions of whole-rock samples were measured using a Shimadzu XRF-1800 sequential X-ray fluorescence spectrometer (XRF) with a voltage of 40 kV and a current of 70 mA at China University of Geosciences (CUG), Wuhan. The measurement procedure and data quality were monitored by replicate analyses of USGS standards BHVO-2 and AGV-2 and the analytical uncertainties are better than 3%. Detailed sample-fusion procedures and analytical precision and accuracy are described by Ma et al. (2012). Trace-element concentrations of whole-rocks were determined at Guangzhou Institute of Geochemistry, Chinese Academy of Sciences (GIGCAS) using a Perkin-Elmer Sciex ELAN 600 inductively coupled plasma-mass spectrometry (ICP-MS) after acid digestion of the samples in high-pressure Teflon bombs, following the analytical procedures described by Liu et al. (1996). Analytical uncertainties are better than 5% for most of measured trace elements and are better than 10% for others (Cr and Pb). Sr and Nd isotopic ratios of whole-rock samples were analyzed using a Micromass Isoprobe Multi-Collector ICPMS after acid digestion at GIGCAS. The measured $^{87}Sr/^{86}Sr$ and $^{143}Nd/^{144}Nd$ ratios were normalized to $^{86}Sr/^{88}Sr = 0.1194$ and $^{146}Nd/^{144}Nd = 0.7219$, respectively. SRM NBS-987, BHVO-2 and La Jolla standard were used to monitor the measurement procedures and data quality. SRM NBS-987 yielded an average $^{87}Sr/^{86}Sr$ of 0.710243 ± 14 (2σ; n = 12). The La Jolla standard measured during the course of analysis yielded an average $^{143}Nd/^{144}Nd$ of 0.511847 ± 3 (2σ; n = 11), and BHVO-2 yielded $^{143}Nd/^{144}Nd$ of 0.512979 ± 6 (2σ; n = 3).

4.2. Mineral major and trace elements

Major- and trace- element compositions of minerals were analyzed at GIGCAS. Major- element compositions of minerals were determined using a JEOL JXA-8100 electron microprobe with an accelerating voltage of 15 kV, a beam current of 20 nA and a beam diameter of 1 ~ 2 μm. *In-situ* trace-element analyses of silicates were carried out by laser ablation (LA)-ICPMS using an Agilent 7500a ICP-MS system coupled with a Resolution M50-HR 193 nm ArF-excimer laser sampler, following the analytical procedures described by Tu et al. (2011). The laser was operated at a repetition rate of 10 Hz, and the spot diameter was 53 μm.

4.3. Zircon U–Pb dating

Cathodoluminescence (CL) images of zircon were obtained prior to secondary ion mass spectrometry (SIMS) and LA-ICPMS analysis, using a Supra 55 Sapphire field emission scanning electron microscope (FESEM) at GIGCAS, to characterize internal structures and to select suitable positions for U–Pb dating analyses. SIMS zircon U–Pb analyses were performed on a Cameca IMS-1280HR ion microprobe at GIGCAS following procedures described by Li et al. (2009). The O_2^- primary ion beam was accelerated at 13 kV, with an intensity of 10 nA. The ellipsoidal spot is about 20 × 30 μm in size. Positive secondary ions were extracted with a 10 kV potential. Calibration of Pb/U ratios is based on an observed linear relationship between $\ln(^{206}Pb/^{238}U)$ and $\ln(^{238}U^{16}O_2/^{238}U)$. A common Pb correction was applied using the measured ^{204}Pb. Analyses of the standards Plesovice and Qinghu were interspersed with unknowns. LA-ICPMS zircon U–Pb isotope analyses were carried on an Agilent 7500a instrument in combination with a Geolas-193 UV laser ablation system at CUG, using a beam diameter of 32 μm. Standards zircon 91500 were used as external standard for calibration. Detailed operating conditions and data reduction for LA-ICPMS zircon U–Pb dating were described by Liu et al. (2010a). Concordia diagrams and weighted mean calculations were made using Isoplot/Ex_ver3 (Ludwig, 2003).

5. Results

5.1. Zircon U–Pb dating

Zircons from a quartz diorite (NC11–40) and a gabbro (CFH11–11) have been used to constrain the emplacement age of the Ningcheng complex. The zircon grains are euhedral, 100–400 μm long and have length/width ratios of 1:1 to 4:1. Most of them show clear oscillatory zoning in CL images (Fig. 3), typical of magmatic zircons. The magmatic zircon grains from quartz diorite NC11–40 yield $^{206}Pb/^{238}U$ ages ranging from 220 to 233 Ma (Table S1), with a weighted mean of 227.4 ± 2.1 Ma (n = 13; MSWD = 0.83), which is interpreted as the crystallization age of the quartz diorite. The magmatic zircon grains from gabbro CFH11–11 yield $^{206}Pb/^{238}U$ ages ranging from 222 to 232 Ma (Table S1), with a weighted mean of 225.7 ± 1.6 Ma (n = 12; MSWD = 1.3), which is interpreted as the crystallization age of the gabbro. Similar late Triassic ages (220 ~ 228 Ma) have also been reported for the Ningcheng complex, defined by U–Pb ages on zircon and baddeleyite from different lithologies (Zhang et al., 2014). We therefore conclude that the Ningcheng complex was emplaced at ~227 Ma and that the gabbros and the quartz diorites are coeval.

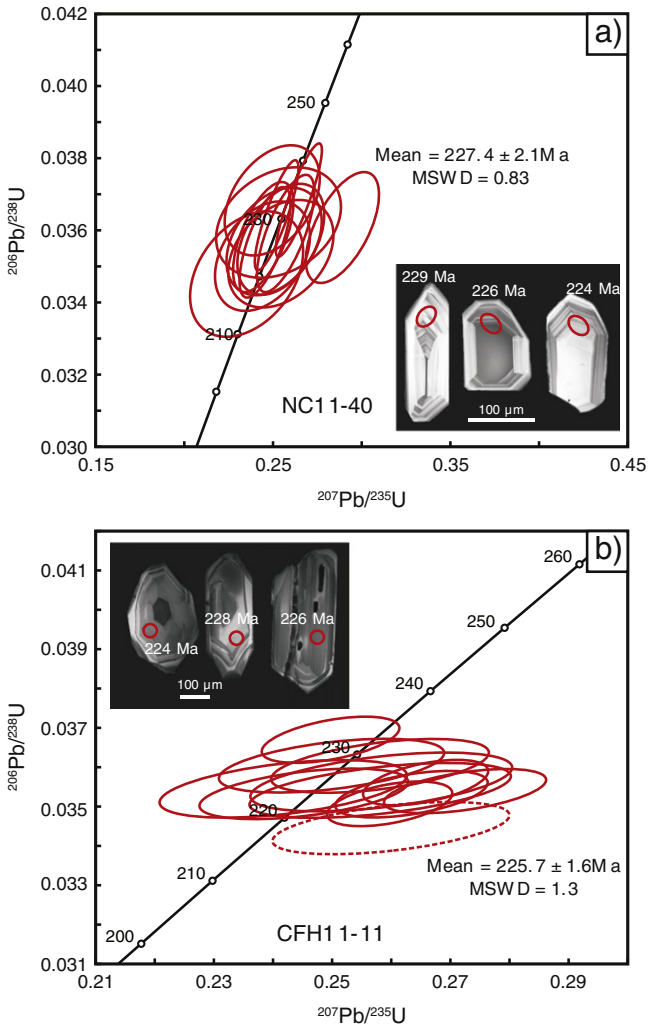

Fig. 3. U–Pb Concordia diagrams and representative cathodoluminescence (CL) images for zircons from the Ningcheng quartz diorite NC11–40 (SIMS) and gabbro CFH11–11 (LA-ICPMS) in the North China Craton.

5.2. Mineral chemistry

The average compositions of minerals from the Ningcheng complex are listed in Table 1, and detailed major- and trace-element compositions of individual minerals are presented in Tables S2-S3.

Euhedral olivine grains are present in ultramafic rocks of the cumulate unit and are interpreted as cumulate crystals. They have variable Fo [Fo = 100 × Mg/(Mg + Fe)] and Ni contents that decrease from high-Mg websterites (Fo = 83.8 to 81.8, Ni = 0.54 to 0.46 wt%) through low-Mg websterites (Fo = 81.5 to 80.3, Ni = 0.25 to 0.19 wt%) to Ol-pyroxenites (Fo = 77.2 to 73.6, Ni = 0.18 to 0.12 wt%) (Fig. 4a).

Pyroxenes are the most important mineral phases of the cumulate unit, and Cpx/Opx ratios increase from the bottom to the top of the sequence. Orthopyroxenes are present as euhedral to subhedral cumulate crystals. They are clinoenstatite ($En_{58.8–84.8}Fs_{12.2–39.2}Wo_{0.7–5.9}$), and Mg# decreases from the high-Mg websterites (~85.2) to the quartz diorites (~61.6) (Fig. 4b). Clinopyroxenes are euhedral to subhedral cumulate crystals and are classified as augite and diopside ($Wo_{32.3–49.0}En_{37.6–56.0}Fs_{8.3–17.6}$) (Morimoto et al., 1988). They display decreasing Mg# and Cr_2O_3 from high-Mg websterites, through low-Mg websterites, Ol-pyroxenites and Hbl-pyroxenites, to gabbros and to quartz diorites (Fig. 4c), i.e. roughly from bottom to top. These clinopyroxenes have variable trace element compositions but do not show systematic differences in their patterns between lithologies. They have convex-upward chondrite-normalized REE patterns with maximum at Nd and are depleted in Nb-Ta-Zr-Hf-Ti relative to neighboring elements in the primitive mantle-normalized trace-element spidergrams (Fig. S1).

Amphibole is absent in the high-Mg websterites and rare (<1 vol%) in the low-Mg websterites and Ol-pyroxenites, whereas it occur as phenocrysts (>10 vol%) or as cumulate minerals (>30 vol%) in the Hbl-pyroxenites and gabbros, respectively. They are classified as magnesiohornblende, magnesiohastingsite and tschermakitic pargasite of the calcic-amphibole group according to the nomenclature of Leake et al. (1997). They have SiO_2, MgO, and FeO of 40.5 ~ 45.6 wt%, 12.6 ~ 16.6 wt% and 8.4 ~ 14.4 wt%, respectively. Remarkably, they have high Al_2O_3 (10 ~ 14.6 wt%), indicative of high pressure crystallization (Ridolfi et al., 2010). Amphiboles from Hbl-pyroxenites and gabbros have similar trace-element compositions with convex upward chondrite-normalized REE patterns and negative anomalies in Th, U, Zr, Hf in the primitive mantle-normalized trace-element plots (Fig. S2).

Plagioclases in the cumulate unit are labradorite and andesine with end-member compositions of $Ab_{39.1–561.9}An_{37.4–60.4}Or_{0.3–3.1}$. Plagioclases in the quartz diorites have lower An contents and are oligoclases with end-member compositions of $Ab_{68.2–77.1}An_{21.0–29.0}Or_{1.5–2.8}$. K-feldspars with end-member compositions of $Ab_{5.8–31.2}An_{0.3–1.7}Or_{67.6–93.9}$ are only present in the quartz diorite unit.

5.3. Whole-rock geochemistry and Sr-Nd isotopes

Whole-rock geochemical compositions and Sr-Nd isotopes of the Ningcheng complex are presented in Tables S4-S5. Major-element compositions are discussed below in terms of wt%, normalized to 100% on a volatile-free basis.

5.3.1. Cumulate unit

Geochemical compositions of the cumulate rocks of the Ningcheng complex are controlled by the modes of their constituent minerals. The ultramafic rocks, including websterites, Ol-pyroxenites and Hbl-pyroxenites, have high MgO (16.0 ~ 30.1 wt%), Fe_2O_3 (7.5 ~ 12.4 wt%), Cr (769 ~ 2930 ppm) and Ni (214 ~ 1290 ppm), low SiO_2 (47.5 ~ 52.9 wt%) and Al_2O_3 (3.5 ~ 10.0 wt%) and high Mg# (75.7 to 84.9) (Figs. 5 and S3), corresponding to high modal abundances of pyroxene, amphibole and olivine (Fig. 2). As mentioned earlier, the websterites are subdivided into a high-Mg (MgO > 26 wt%) and a low-Mg group (MgO < 20 wt%). The former have higher Fe_2O_3 and Ni contents and Mg# but lower Al_2O_3 and CaO contents (Fig. 5) than the latter in accord with their different Cpx/Opx modal ratios. These ultramafic rocks have variable incompatible-element compositions that show minor differences among them. In the chondrite-normalized rare-earth element diagram (Fig. 6a), the high-Mg websterites and Ol-pyroxenites show an enrichment of light rare earth elements (LREEs) over heavy rare earth elements (HREEs) with negligible Eu anomalies. In contrast, the low-Mg pyroxenites and Hbl-pyroxenites have convex-upward chondrite-normalized REE patterns with the maximum at Nd and show fractionation of middle *vs* heavy rare earth elements. All the ultramafic rocks are enriched in LREEs, large-ion lithophile elements (LILEs; such as K, Rb, Ba and/or Th) and Pb, with negative anomalies in high-field-strength elements (HFSEs; such as Nb, Ta and/or Ti) in the primitive mantle-normalized trace-element diagrams (Fig. 6b).

The mafic rocks range in composition from gabbro to gabbroic diorite (Fig. 5c) with SiO_2 of 50.9 ~ 53.9 wt% and total alkalies ($Na_2O + K_2O$) of 2.8 ~ 5.0 wt%. They also have high (but lower than those of ultramafic rocks) MgO (4.2 ~ 8.6 wt%), Fe_2O_3 (5.3 ~ 12.1 wt%), Cr (63 ~ 124 ppm), Ni (41 ~ 224 ppm) and Mg# (52.3 ~ 74.4) (Figs. 5 and S3). Compared to the ultramafic rocks, these gabbros have obviously higher Al_2O_3 contents (Fig. 5d) and lower CaO/Al_2O_3 (Fig. S3c)

Table 1
Average compositions (wt%) of minerals from Ningcheng complex in the North China Craton.

Rock	high-Mg websterite				low-Mg websterite						Ol-pyroxenite					
Sample	NC1113–1				NC1108–2 & NC1107–2						CFH11–9					
Mineral	Ol	Opx	Cpx	Bi	Ol	Opx	Cpx	Am	Bi	Pl	Ol	Opx	Cpx	Am	Bi	Pl
Number	n = 7	n = 12	n = 5	n = 8	n = 4	n = 10	n = 10	n = 6	n = 4	n = 10	n = 5	n = 5	n = 6	n = 3	n = 3	n = 3
SiO_2	38.62	54.51	52.11	39.14	40.40	53.59	50.63	42.06	37.72	53.82	37.41	54.84	51.33	43.02	38.63	51.16
TiO_2	0.06	0.18	0.50	3.98	0.02	0.24	0.64	2.83	5.12	0.08	0.05	-	0.77	0.84	2.32	0.07
Al_2O_3	0.01	2.08	3.49	16.08	0.01	3.47	4.59	13.44	15.87	29.00	0.01	1.21	3.41	11.92	16.54	29.45
Cr_2O_3	0.04	0.46	0.74	0.71	-	0.29	0.48	0.66	0.72		0.06	0.10	0.43	0.29	0.68	
FeO	16.26	9.70	5.90	7.13	17.26	12.45	6.41	9.00	8.94	0.13	22.46	13.31	6.87	10.18	8.32	0.15
MnO	0.21	0.19	0.12	0.04	0.17	0.23	0.14	0.12	0.03		0.29	0.33	0.16	0.11	0.05	
MgO	44.78	31.29	17.52	20.70	41.28	28.53	15.14	14.19	18.81	0.01	40.15	28.97	16.20	16.12	20.71	0.01
CaO	0.01	1.20	18.90	-	0.00	1.41	20.95	11.73	0.01	11.01	<0.01	1.14	20.72	11.35	0.01	12.96
Na_2O	-	0.09	0.93	0.80	-	0.06	0.74	2.48	0.35	6.07	-	0.04	0.72	3.19	1.21	4.92
K_2O	-	0.01	0.01	9.47	-	0.01	0.01	1.41	9.93	0.21	-	0.01	0.01	1.01	9.24	0.09
NiO	0.51	0.12	0.07		0.22	0.07	0.04				0.14	0.03	0.02			
P_2O_5	-	0.02	0.03	0.02	-	0.02	0.03	0.07	-		-	0.02	0.03	0.04	-	
Total	100.44	99.77	100.28	98.04	99.37	100.34	99.76	97.92	97.50	100.27	100.52	100.02	100.62	98.05	97.70	98.80
Mg#	83.1	85.2	84.2	83.7	81.0	80.3	80.9	73.8	78.9		76.1	79.5	80.9	73.8	81.6	
En		0.83	0.51			0.78	0.45					0.77	0.46			
Fs		0.15	0.10			0.19	0.11					0.20	0.11			
Wo		0.02	0.39			0.03	0.44					0.02	0.43			
Ab										49.3						40.5
An										49.6						59.0
Or										1.1						0.5
T-PKD	1112 °C				991–1027 °C						1019 °C					
P-PKD	6.8 kbar				5.3–6.2 kbar						5.9 kbar					
P-HZ					7.7 kbar						6.2 kbar					
P-Hgea					8.3 kbar						6.6 kbar					
P-SMW					8.0 kbar						6.5 kbar					
P-AS					8.0 kbar						6.5 kbar					

Rock	Hbl-pyroxenite				gabbro				quartz diorite					
Sample	NC11–12				NC1110–2				NC11–34 & NC11–40					
Mineral	Opx	Cpx	Am	Pl	Opx	Cpx	Am	Pl	Opx	Cpx	Am	Bi	Pl	Kfs
Number	n = 8	n = 7	n = 7	n = 2	n = 3	n = 8	n = 10	n = 8	n = 3	n = 6	n = 5	n = 14	n = 13	n = 8
SiO_2	53.27	51.45	42.46	55.47	53.62	51.32	41.27	54.69	51.48	52.24	44.03	38.16	60.10	64.06
TiO_2	0.24	0.65	3.84	0.07	0.33	0.58	4.45	0.08	0.28	0.34	1.78	4.65	0.05	0.03
Al_2O_3	2.10	3.56	12.47	26.42	2.57	2.92	12.49	27.99	0.60	1.44	10.18	13.65	23.88	18.58
Cr_2O_3	0.09	0.16	0.20		0.03	0.09	0.06		0.02	0.03	0.06	0.10		
FeO	15.38	8.37	10.60	0.12	16.68	8.73	11.79	0.19	23.82	10.18	13.65	17.81	0.19	0.11
MnO	0.40	0.26	0.12		0.38	0.28	0.14		0.66	0.36	0.21	0.14		
MgO	26.75	14.84	13.32	-	24.42	15.10	13.03	0.01	21.48	13.53	13.92	13.61	0.01	-
CaO	1.30	20.21	11.21	9.30	1.21	20.71	11.28	10.30	1.22	21.64	11.33	0.03	5.97	0.22
Na_2O	0.05	0.83	2.63	7.28	0.14	0.63	2.84	6.63	0.02	0.62	1.98	0.11	9.63	2.06
K_2O	-	-	1.23	0.40	-	-	1.38	0.33	0.02	0.01	1.23	10.45	0.42	15.39
NiO	0.03	0.03			-	0.02			0.02	0.03				
P_2O_5	0.01	0.04	-		0.04	0.03	0.05		0.01	0.03	0.02	0.01		
Total	99.60	100.37	98.09	99.08	99.38	100.39	98.72	100.22	99.60	100.42	98.37	98.72	100.24	100.46
Mg#	75.6	76.1	69.1		72.3	75.7	66.3		61.6	70.3	64.5	57.6		
En	0.73	0.43			0.70	0.43			0.60	0.39				
Fs	0.24	0.14			0.27	0.14			0.38	0.17				
Wo	0.03	0.42			0.02	0.42			0.02	0.44				
Ab				57.4				52.8					72.9	16.7
An				40.5				45.4					25.0	1.0
Or				2.1				1.8					2.1	82.4
T-PKD	983 °C				1033 °C									
P-PKD	5.4 kbar				5.3 kbar									
P-HZ	6.9 kbar				7.0 kbar				4.9 kbar					
P-Hgea	7.4 kbar				7.5 kbar				5.1 kbar					
P-SMW	7.3 kbar				7.3 kbar				5.3 kbar					
P-AS	7.3 kbar				7.3 kbar				5.3 kbar					

Mineral abbreviations: Ol, olivine; Opx, orthopyroxene; Cpx, clinopyroxene; Am, amphibole; Bi, biotite; Pl, plagioclase.
Mg# = 100 × Mg/(Mg + Fe), where Mg and Fe represent molar proportions.
T-PKD and P-PKD are calculated by two-pyroxene thermometers and barometers (Putirka, 2008).
P-HZ, P-Hgea, P-SMW and P-AS are calculated by Al in amphibole barometeric equations from Hammarstrom and Zen (1986), Hollister et al. (1987), Schmidt (1992) and Anderson and Smith (1995), respectively.

because of the high modal abundance of plagioclase. They show enrichment of LREEs over HREEs with negligible to positive Eu anomalies (δ_{Eu} = 1.0 to 1.6) (Fig. 6c). They are enriched in LREEs, LILEs, with negative anomalies in HFSEs (Fig. 6d). They are characterized by high Sr (≥1000 ppm) and LREEs, low Y (≤17 ppm) and HREEs (Yb ≤ 1.4 ppm), and high Sr/Y (≥60) and La/Yb (≥8.6) (Fig. 7).

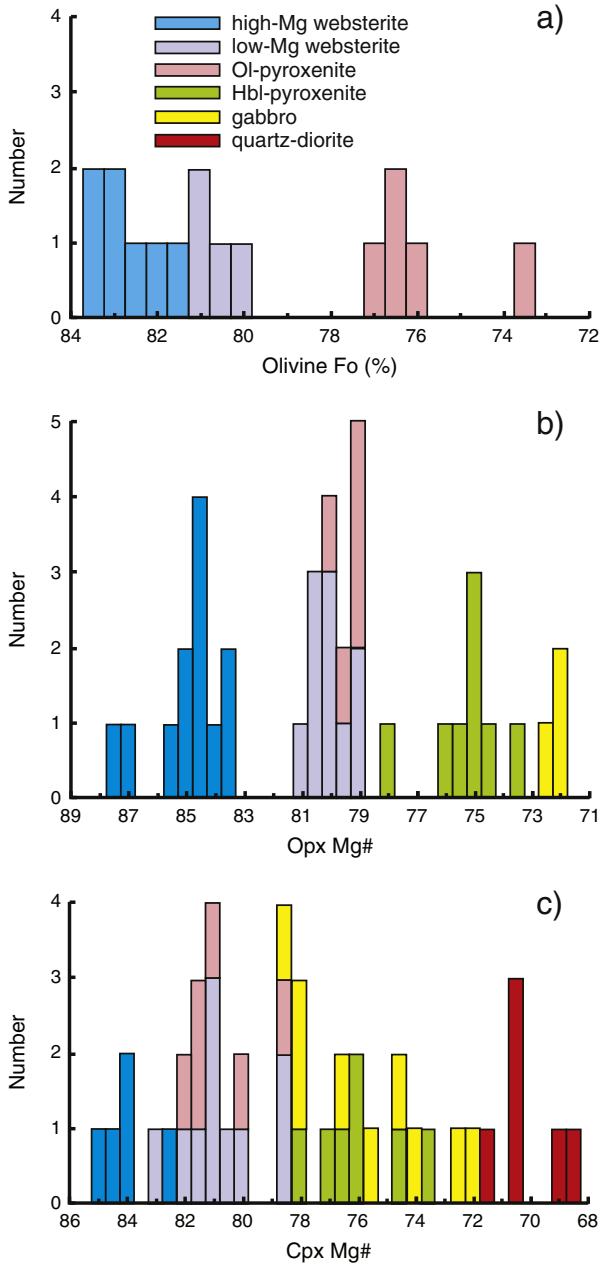

Fig. 4. Comparisons of Fo contents of olivines and Mg-numbers (Mg# = 100 × Mg/(Mg + Fe)) of pyroxenes in different units of Ningcheng Complex in the North China Craton.

The initial $^{87}Sr/^{86}Sr$ ratios and $\varepsilon_{Nd}(t)$ values have been calculated at 227 Ma, corresponding to the zircon and baddeleyite U–Pb ages of the Ningcheng complex. The Sr-Nd isotopic compositions of the ultramafic-mafic rocks are relatively homogeneous with $(^{87}Sr/^{86}Sr)_i$ of 0.7055 to 0.7067 and negative $\varepsilon_{Nd}(t)$ values of −1.7 to −6.3 (Table S5; Fig. 8). There are no systematic differences in isotopes between lithologies; the isotopic values are comparable with those of early Mesozoic subcontinental lithospheric mantle (SCLM) beneath the NCC (Yang et al., 2009; Zhang et al., 2008; Zheng and Lu, 1999).

5.3.2. Quartz diorite unit

The quartz diorites range in composition from monzonite to quartz monzonite (Fig. 5c) with SiO_2 of 57.0 ~ 62.9 wt% and total alkalies ($Na_2O + K_2O$) of 6.9 ~ 8.8 wt%. Compared to the coexisting cumulate rocks, these rocks have lower MgO (2.9 ~ 3.6 wt%), Fe_2O_3 (4.7 ~ 5.8 wt%), Ni (26 ~ 85 ppm) and Cr (32 ~ 65 ppm) (Fig. 5), and higher levels of incompatible trace elements (Fig. 6e-f). They also have high Al_2O_3 (15.2 ~ 20.4 wt%) and low CaO (3.6 ~ 5.4 wt%). The quartz diorites are characterized by adakitic signatures (Ma et al., 2015) with high Sr (≥636 ppm) and LREEs, low Y (≤17 ppm) and HREEs (Yb ≤ 1.8 ppm), a lack of obvious Eu anomalies (Fig. 6e), and high Sr/Y (≥31) and La/Yb (≥24) (Fig. 7). All these features are broadly similar to those of modern adakites (Defant and Drummond, 1990), Archean TTG suites (Martin et al., 2005), and experimental melts of a mafic lower crust at pressures of 10 to 12.5 kbar (Qian and Hermann, 2013). These rocks are enriched in LREEs, LILEs (e.g. Rb, Ba and Th) and Pb, with negative anomalies in HFSEs (Fig. 6f). Two samples (NC11–17 and CFH11–11), which have the lowest SiO_2 (57.0 wt% and 58.6 wt%) of this unit, show positive Eu anomalies and depletion in Th-U relative to Rb-Ba (Fig. 6e, f), consistent with plagioclase accumulation in their petrogenesis.

The quartz diorites have Sr-Nd isotopic compositions with $(^{87}Sr/^{86}Sr)_i$ of 0.7060 to 0.7067 and negative $\varepsilon_{Nd}(t)$ values of −5.3 to −3.9 (Table S5). The data mostly overlap with those of the cumulates (Fig. 8).

6. Discussion

6.1. Crystallization pressure and temperature

Al-in-hornblende barometers (Anderson and Smith, 1995; Hammarstrom and Zen, 1986; Hollister et al., 1987; Schmidt, 1992)) and a two-pyroxene thermobarometer (Putirka, 2008) have been used to estimate the crystallization pressure and temperature of the Ningcheng complex (Table 1 and Fig. 2).

The two-pyroxene thermobarometer suggests that the high-Mg websterites record a crystallization at high temperature (~1112 °C) and deep-crustal depths (~6.8 kbar). The high temperature estimates are also supported by the absence of cumulate amphibole and the high pressure is in agreement with the pyroxene-dominated cumulate assemblages (Blatter et al., 2013; Müntener et al., 2001).

Pressures (5.3 ~ 6.2 kbar) and temperatures (983 ~ 1027 °C) calculated by the two-pyroxene thermobarometer are virtually identical for the low-Mg websterites, Ol-pyroxenites and Hbl-pyroxenites. These estimates are slightly shallower and colder than those of the high-Mg websterites. The crystallization pressures estimated by Al-in-hornblende barometers are higher than those of the two-pyroxene thermobarometry, ranging from ~6.2 kbar for the Ol-pyroxenites to ~8.3 kbar for the low-Mg websterite.

The compositions of clino- and ortho-pyroxenes from the Ningcheng gabbros record a high crystallization temperature of ~1033 °C like those of the underlying low-Mg websterites, and a crystallization pressure of ~5.3 kbar which is shallower than those of the underlying low-Mg websterites. The crystallization pressure estimated by Al-in-hornblende barometers ranges between 7.0 and 7.5 kbar, also lower than those of the underlying low-Mg websterites but consistent with those of Ol-pyroxenites and Hbl-pyroxenites.

The lack of coexisting clinopyroxene and orthopyroxene in the quartz diorites does not permit temperature estimation. We have only estimated their crystallization pressure using the Al-in-hornblende barometers, which yield estimates of 4.9 to 5.3 kbar. These pressure estimates are obviously lower than those of the coexisting cumulate unit.

In summary, the application of different barometers suggests that the Ningcheng complex was emplaced at mid- to lower-crustal depths (4.9 ~ 8.3 kbar) with crystallization pressures decreasing from the bottom (high-Mg websterite) to the top (quartz diorite) (Fig. 2). Along with the apparent decrease in pressure, the rocks from the cumulate unit record a rough trend of crystallization temperatures decreasing from the bottom to the top of the sequence.

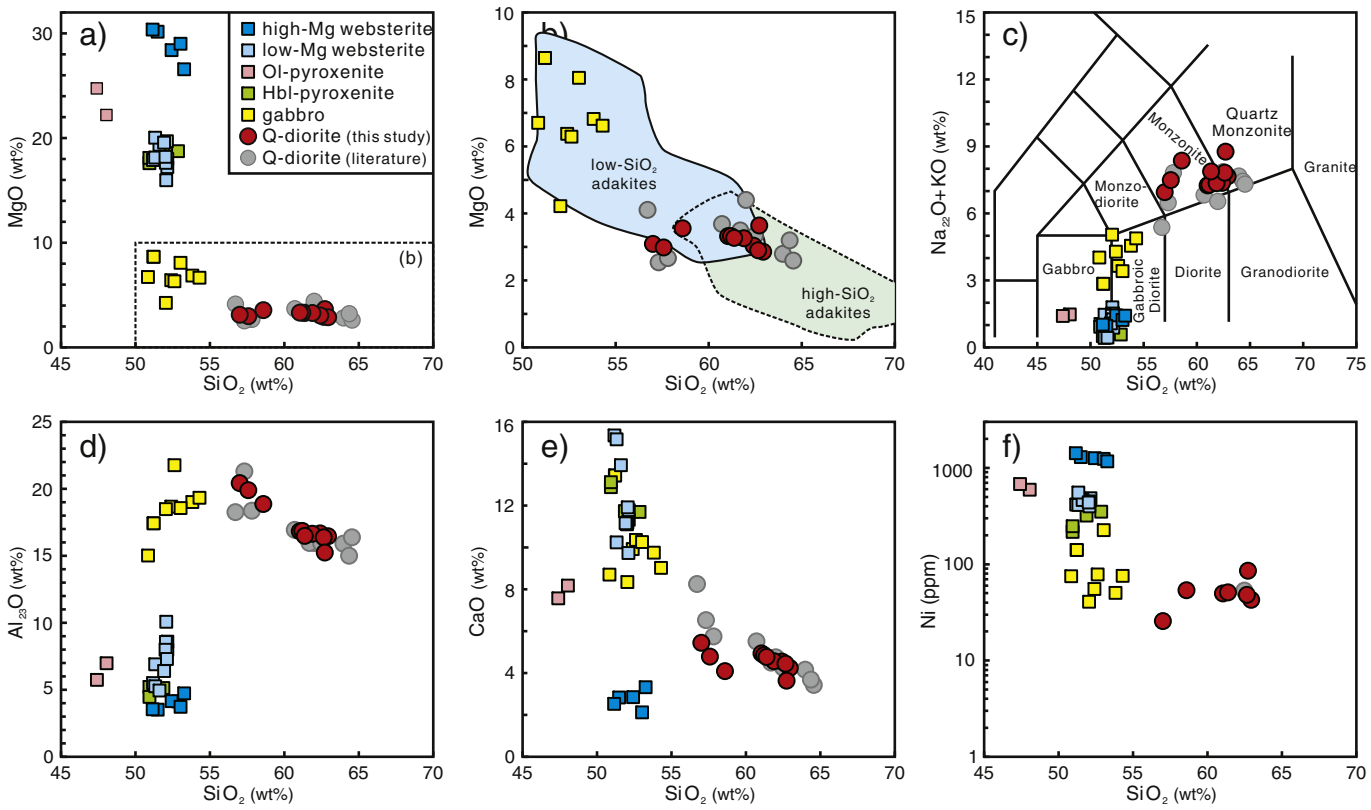

Fig. 5. Plots of (a-b) MgO, (c) $Na_2O + K_2O$, (d) Al_2O_3, (e) CaO and (f) Ni *vs* SiO_2 for Ningcheng complex in the North China Craton. Oxide compositions of whole-rocks have been recalculated to 100% on an anhydrous basis. Data for quartz diorites are from Han et al. (2000), Zhang et al. (2014) and this study.

6.2. Crystal fractionation sequence in the Ningcheng complex

It is clear from the field relationships, petrography, mineral compositions and whole-rock geochemical variations that the Ningcheng websterites-(Ol−/Hbl-)pyroxenites-gabbros and quartz diorites represent the cumulates and complementary derivative magmas, respectively, from one or several similar parental magmas. The crystal fractionation sequence of the Ningcheng complex can be determined from the cumulate (exclusive of interstitial) minerals in the cumulate rocks and the mineral assemblages of the quartz diorites.

The earliest stage of fractionation of the magma was dominated by crystallization of Opx + Cpx ± Ol with a low Cpx/Opx ratio, represented by the high-Mg websterite at the bottom of the cumulate unit. The crystallizing silicate minerals display the highest Mg# (as well as high Ni or Cr contents) of all cogenetic minerals in the Ningcheng complex (Fig. 4). Hydrous minerals (e.g. amphibole) are absent in this stage, probably because of the high temperature of the magmas (~1112 °C); hydrous minerals are not stable on the liquidus of such magmas at temperature greater than about 1050 °C (Blatter et al., 2013; Müntener et al., 2001).

An intermediate stage is also dominated by growth of orthopyroxene and clinopyroxene, manifested by the low-Mg websterites, Ol-pyroxenites and Hbl-pyroxenites. However, this stage is characterized by higher Cpx/Opx ratios than the earlier stage and the presence of amphibole (Fig. 2). With decreasing temperature (from ~ 1112 °C for the high-Mg websteritic stage to <1027 °C for this stage), clinopyroxene crystallized at the expense of orthopyroxene, resulting in lower MgO and higher CaO in the low-Mg websterites. The observed fractionation sequence is consistent with high-pressure crystallization of hydrous magmas, in which Cpx/Opx ratios increase with decreasing temperature and/or with increasing H_2O in the melt (Müntener et al., 2001). The appearance of amphibole suggests that the magma was hydrous with temperatures <1050 °C at this stage.

In the later differentiation of the magma, crystallization produced assemblages with higher proportions of plagioclase and amphibole and a lower proportion of clinopyroxene (i.e. hornblende gabbro). Accordingly, with increasing mode of plagioclase and decreasing mode of Fe-Mg silicates, whole rock compositions become higher in Al_2O_3 and lower in MgO, Fe_2O_3, Cr, Ni and Mg# (Figs. 5 and S3).

Crystallization of the cumulate unit drove the derivative melts towards high Si, and low Mg, Fe and Ca, comparable with compositions of the quartz diorites. Considering the field relationships, petrography and whole-rock compositions, the quartz diorites are interpreted as solidified residual melts derived from fractional crystallization of the basalt/basaltic andesite (see discussion below). Therefore, the mineral assemblage of the quartz diorites (Pl + Bi + Q ± Hbl ± Kfs ± Cpx) represents the final crystallized phases.

To summarize the above discussion, we can define the following crystallization sequence for the Ningcheng complex:

$$\text{Opx} + \text{Cpx} \pm \text{Ol} \rightarrow \text{Opx} + \text{Cpx} + \text{Hbl} \pm \text{Ol} \pm \text{Pl} \rightarrow \text{Pl} + \text{Cpx} + \text{Hbl} \pm \text{Opx} \rightarrow \text{Pl} + \text{Bi} + \text{Q} \pm \text{Hbl} \pm \text{Kfs} \pm \text{Cpx} \quad \text{(i)}$$

or simply as

$$\text{Opx} + \text{Cpx} \rightarrow \text{Hbl} \rightarrow \text{Pl} \rightarrow \text{Bi} + \text{Q} \pm \text{Kfs} \quad \text{(ii)}$$

to emphasize the onset of crystallization of each phase.

6.3. Nature of the parental magma

6.3.1. A basalt/basaltic andesite parental magma

The high-Mg websterites formed in the earliest stage of fractionation of the magma, which makes them the ideal subject for constraining the nature of their parental magma (or starting composition). The

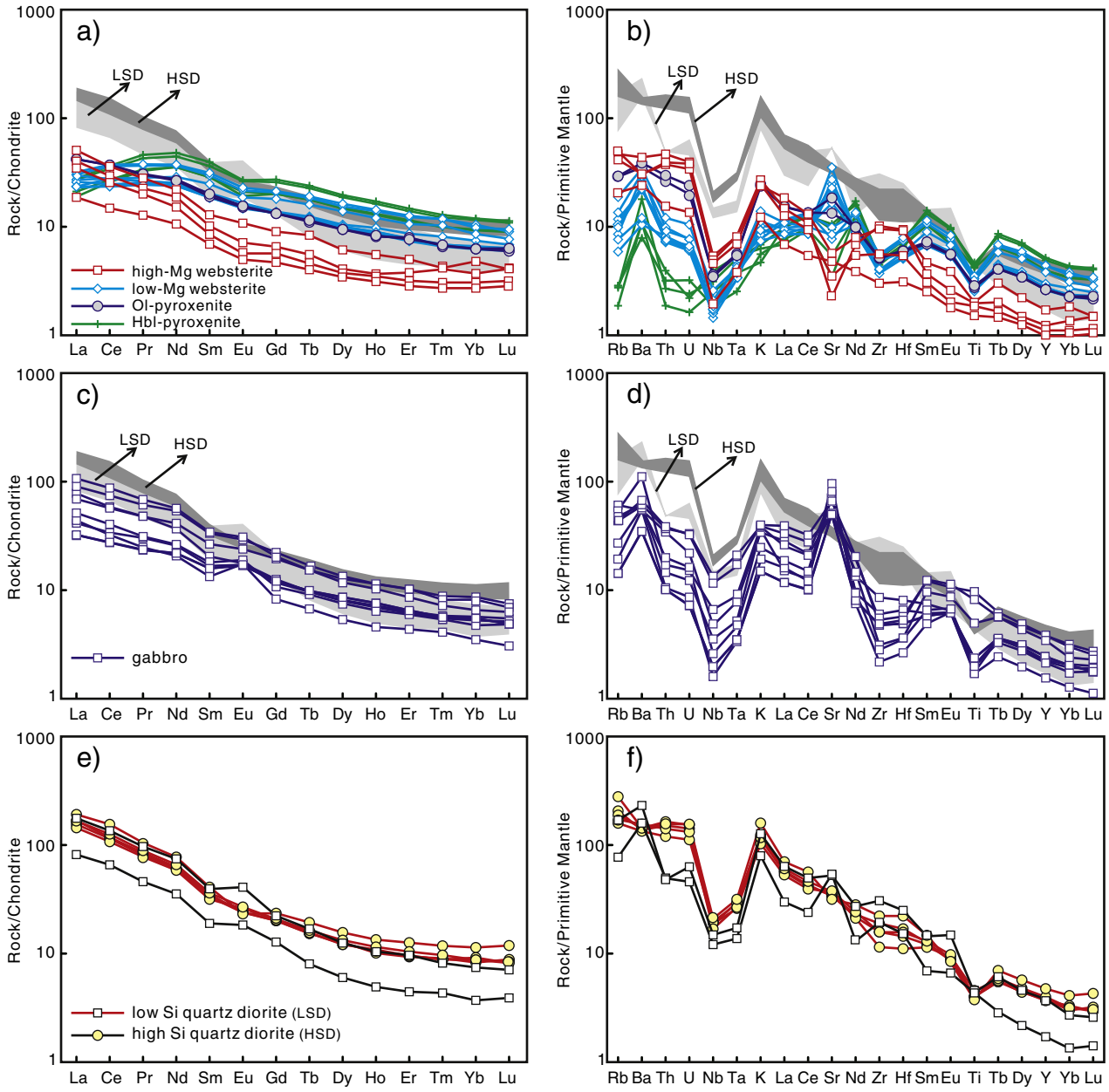

Fig. 6. Chondrite-normalized REE patterns (a, c and e) and primitive mantle-normalized trace-element patterns (b, d and f) for the Ningcheng complex in the North China Craton. HSD, high-Si quartz diorite with SiO_2 > 58 wt%; LSD, low-Si quartz diorite with SiO_2 < 58 wt%. Normalizing values are from McDonough and Sun (1995).

cumulate silicates in the high-Mg websterites are magnesian with Mg# (or Fo) of ~83.1, ~85.2 and ~84.2 for olivines, orthopyroxenes and clinopyroxenes, respectively. If we assume that these minerals were in equilibrium with the magma from which they precipitated, we can calculate the Mg# of the melts using available Mg-Fe partition coefficients [$K_D^{Fe\text{-}Mg} = (Mg^{liq}Fe^{mineral})/(Mg^{mineral}Fe^{liq})$]. Clinopyroxene is not taken into account in the calculations because the $K_D^{Fe\text{-}Mg}$ between clinopyroxene and mafic melt is less well constrained than those for olivine-melt (0.30 ± 0.03; Roeder and Emslie, 1970) and orthopyroxene-melt (0.255 ~ 0.29; Putirka, 2008; Straub et al., 2008). The results show that a nominal coexisting liquid would be mafic with Mg# varying from 58 to 68 depending on the choice of $K_D^{Fe\text{-}Mg}$ values (Table S2). Considering the effect of trapped-liquid crystallization on cumulus mineral compositions (Barnes, 1986), these calculated Mg numbers represent minimum estimates for that of the actual coexisting magma. Thus we conclude that the parental magma of the Ningcheng complex was mafic with a basaltic or basaltic-andesitic composition; that is, they were derived from the mantle rather than a mafic crust source. This argument is also supported by the relatively low SiO_2 (lack of granodiorite and granite in the complex) and high MgO and Mg# of the quartz diorites (Fig. 5), which cannot form by simple differentiation from a crustal derived melt (Lee et al., 2014; Martin et al., 2005; Qian and Hermann, 2013). The fact that all quartz diorites have initial Sr-Nd isotopes different from the lower crustal rocks of the NCC (Fig. 8) further argues against a parental magma derived from the lower crust.

6.3.2. A hydrous parental magma

H_2O is a crucial component in the fractionation sequence of basaltic and basaltic andesitic magmas (Blatter et al., 2013; Gaetani et al., 1993; Müntener et al., 2001). At crustal pressures, a low H_2O concentration in the liquid stabilizes plagioclase earlier than pyroxene and amphibole, which results in crystallization being dominated by olivine + plagioclase. Increasing H_2O concentration in the liquid suppresses plagioclase crystallization (Gaetani et al., 1993; Müntener et al., 2001) thereby

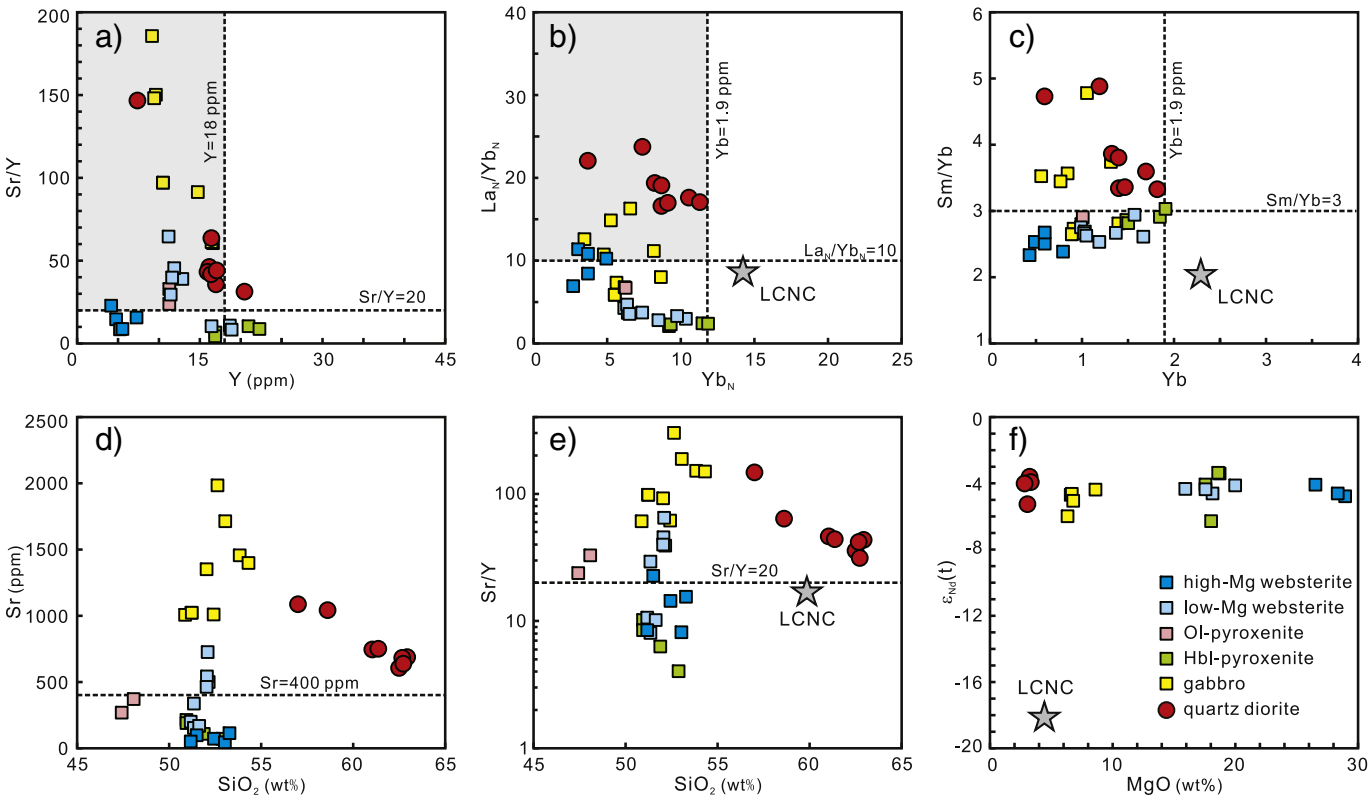

Fig. 7. Plots of Sr/Y *vs* Y (a), $(La/Yb)_N$ *vs* Yb_N (b), Sm/Yb *vs* Yb (c), Sr *vs* SiO_2 (d), Sr/Y *vs* SiO_2 (e) and $\varepsilon_{Nd}(t)$ *vs* MgO (f) for Ningcheng complex in the North China Craton. Data for the lower crust of the NCC (LCNC) are from Gao et al. (1998) and Jiang et al. (2013).

producing pyroxenite-dominated cumulate assemblages. As mentioned before, the differentiation of the Ningcheng melts followed a path of websterites-(Ol−/Hbl-)pyroxenites-gabbros in terms of mineral assemblage, comparable with the solid assemblages left by fractional crystallization of hydrous magmas (Blatter et al., 2013; Müntener et al., 2001; Nandedkar et al., 2014) and cumulates from hydrous arc magmas (Jagoutz et al., 2011) at lower-crustal levels. Plagioclase is absent from the cumulus assemblage of the high-Mg websterites (early fractionation stage), low-Mg websterites and Hbl-pyroxenites (intermediate fractionation stage), and is present in higher proportions during the late differentiation of the magma. Therefore, we suggest that the cumulate unit of the Ningcheng complex records a typical hydrous, high-pressure fractionation sequence. Moreover, the inferred liquid line of descent, with the early appearance of amphibole and the late appearance of plagioclase, also is typical for high-pressure fractionation of parental melts with high initial water contents (at least ≥2 wt%) (Blatter et al., 2013; Jagoutz et al., 2011; Müntener et al., 2001). We thus propose that the parental magma of the Ningcheng complex was hydrous.

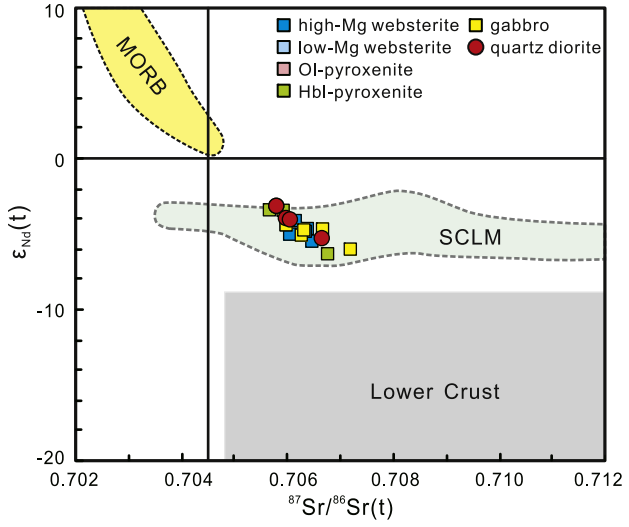

Fig. 8. Whole-rock Sr-Nd isotopic compositions of Ningcheng complex in the North China Craton. Field of Sr-Nd isotopes of MORBs in (a) is after *http://www.earthchem.org/petdb*. Subcontinental lithospheric mantle (SCLM) beneath the NCC is represented by peridotite xenoliths and perovskite from the Paleozoic kimberlites (Zheng and Lu, 1999; Zhang et al., 2008; Yang et al., 2009). Lower crust beneath the NCC is from Jiang et al. (2013).

6.3.3. An enriched subcontinental lithospheric mantle source

The trace-element compositions of the cumulus clinopyroxenes and amphiboles in the cumulate rocks provide further constraints on the nature of their parental magma. Incompatible trace element compositions of melts in equilibrium with these silicate minerals were calculated using experimentally determined mineral-melt partition coefficients (Table S6). Although the modelled melts have variable trace element compositions depending on the minerals in different host lithologies and the selected partition coefficients (Figs. S1 and S2), they show similar patterns, consistent with those of the quartz diorites (Fig. 9). These hypothetical melts and the quartz diorites have fractionated REE patterns with negligible Eu anomalies. They are enriched in LREEs, LILEs and Pb, and are depleted in HFSEs. Such island arc-type trace element patterns in basalts and basaltic andesites are attributable to the involvement of recycled crustal components in the mantle source (Grove et al., 2002) or partial melting of enriched lithospheric mantle (Pallares et al., 2008; Xu et al., 2004). Geological observations suggest that the northern part of the NCC was tectonically in a post-collisional extensional regimes in the early Mesozoic (Ma et al., 2012) after the final closure of the Palaeo-Asian Ocean at 300–250 Ma (Xiao et al., 2003). The crustal components (high LREEs, LILEs and H_2O) in the Ningcheng magmas are unlikely to be derived from subducted materials, given the lack of contemporaneous subduction in the region. A more reasonable scenario

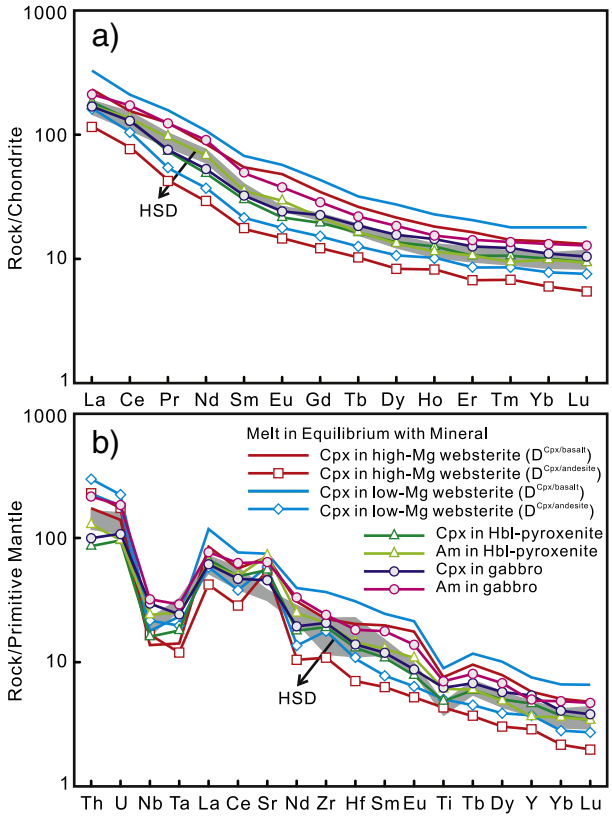

Fig. 9. Chondrite-normalized REE patterns (a) and primitive mantle-normalized trace-element patterns (b) for hypothetical liquids in equilibrium with clinopyroxenes and amphiboles from Ningcheng cumulates. These plots only present the average compositions of calculated liquids. Detailed compositions of individual minerals and their corresponding equilibrated liquids are present in Figs. S1 and S2. Partition coefficients used in modeling are listed in Table S6.

is that the Ningcheng magmas were derived from a phlogopite-rich mantle source (Fig. S4) which had been metasomatized previously and therefore was enriched in incompatible trace elements.

Evidence for an enriched mantle source also comes from the whole-rock Sr-Nd isotopic data. The Ningcheng complex has a Sr-Nd isotopic signature of enriched continental lithosphere with initial $^{87}Sr/^{86}Sr$ ratios of 0.7055 to 0.7072 and negative $\varepsilon_{Nd}(t)$ values of −1.7 to −6.3 (Fig. 8). There are two possible source reservoirs that can produce this enriched isotopic signature: enriched lithospheric mantle and lower continental crust, or a mixture of these two reservoirs. However, in the plot of initial Sr-Nd isotopes (Fig. 8), the Ningcheng igneous rocks are isotopically distinct from the field of lower continental crust as defined by locally-derived xenoliths, and overlap with those of early Mesozoic SCLM beneath the NCC.

We therefore consider that the parental magma of the Ningcheng complex is a hydrous basalt or basaltic andesite, which was derived from partial melting of the enriched lithospheric mantle beneath the NCC.

6.4. Petrogenesis of the Ningcheng high-Mg adakitic plutons

The above described major- and trace-element characteristics of the Ningcheng quartz diorites are broadly similar to the high-Mg (or high-Mg#) adakitic rocks (Gao et al., 2004), low-silica adakites and Archean sanukitoids/TTGs (Martin et al., 2005). The adakitic trace elements and magnesian signatures of high-Mg adakitic rocks are commonly regarded as the products of interaction between high-Sr/Y felsic magmas and mantle peridotites or mantle-derived basalts. However, results of our study indicate a different petrogenetic evolution for the Ningcheng high-Mg adakitic plutons.

Various models have been proposed to account for the origin of igneous rocks with adakitic trace element signatures (Castillo, 2012; Ma et al., 2015; Moyen, 2009), including partial melting of subducted oceanic crust (Defant and Drummond, 1990) or thickened/foundered mafic lower crust (Atherton and Petford, 1993; Gao et al., 2004) with an emphasis on high-pressure melting, partial melting of ancient lower continental crust with the emphasis on source inheritance (Ma et al., 2012, 2015; Qian and Hermann, 2013), and compositional evolution of magma chambers including fractional crystallization (and crustal assimilation) processes in basaltic magmas and mixing between basaltic and felsic magmas (Castillo et al., 1999; Guo et al., 2007; Lee et al., 2007; Richards and Kerrich, 2007). In the previous section, it was shown that most probable source of the parental magmas of the Ningcheng complex is an enriched SCLM, making the slab melting and lower crust melting models unlikely in the Ningcheng case.

Assimilation of crustal rocks is common during the evolution of magmas in a continental setting. However, the Ningcheng complex has homogeneous and obviously higher initial Nd isotopic compositions than the lower crust in the NCC (Fig. 7f), which suggests that the proportion of assimilated material should be limited. Moreover, the lower crust of the NCC has higher HREEs and Y, but lower La/Yb, Sm/Yb and Sr/Y than the Ningcheng adakitic plutons (Fig. 7), indicating that assimilation processes would only have played a limited role in generating adakitic geochemical signatures.

Crystal fractionation/accumulation was the principal process in generating the Ningcheng complex. The gabbroic cumulates (SiO_2 = 50.9–54.3 wt%) are rich in Sr (>1000 ppm; Fig. 7d) and have high Sr/Y ratios (60 ~ 297) due to plagioclase accumulation. Unlike these gabbros, the adakitic quartz diorites are solidified derivative melts with moderate SiO_2 (57.0 ~ 62.9 wt%). It is clear that the websterite-(Ol−/Hbl-)pyroxenite cumulates and quartz diorites are complementary, with their combined compositions reproducing the compositions of late Mesozoic hydrous mafic magmas from the NCC (Fig. 10). The early-crystallizing phases from the Ningcheng magmas, represented by websterites and pyroxenites, have low Sr and LREE (Figs. 6a, 7d and 10). So the fractionation of these minerals results in increasing Sr/Y, La/Yb and Sm/Yb ratios in the derivative melts (Figs. 7a-c and 10) before plagioclase and apatite occur as liquidus phases along the liquid line of descent. The quartz diorites have high Al_2O_3 and P_2O_5 contents (Fig. 5d) due to the absence of plagioclase and apatite during the early differentiation of the magmas. However, the two quartz diorite samples (NC11–37 and CFH11–11) which have the lowest SiO_2 (57.0 wt% and 58.6 wt%) in this unit, have positive Eu anomalies and are relatively depleted in Th-U (Fig. 6), a feature that cannot be explained solely by the removal of cumulates. One possible interpretation is that the magma solidified rapidly without efficient separation of early-crystallized plagioclase and melts (i.e. mushy, crystal-rich magma system) in the lower part of the magma mush. At a given SiO_2, the Ningcheng quartz diorites have higher Mg# than adakitic melts directly derived from basaltic sources. This could be due to one of the following reasons, which are not mutually exclusive: 1) fractionation of magnetite and ilmenite drives the derivative melts towards lower FeO contents at a given MgO; 2) clinopyroxene-dominated rather than olivine-dominated solid assemblages retard the Mg-depletion of derivative liquids, producing melts with relatively high Mg#; 3) magmatic recharge or mixing with basaltic liquids would elevate their Mg number (Lee et al., 2014); 4) they inherited high Mg/Si from the parental magma if it was s high-Mg andesite.

Finally, the low HREEs and Y in adakitic rocks and TTGs are commonly interpreted as indicative of the involvement of garnet as residual or fractionating phase during magma genesis (Moyen, 2009). However, no garnet is observed in the Ningcheng cumulates. As shown in Fig. 7, all the lithologies of the Ningcheng complex have low HREEs and Y regardless of whether they are cumulates or derivative magmas, suggesting that their parental magmas were also intrinsically deficient in these trace elements and the adakitic rocks inherited such compositional characteristics. As mentioned before, the parental magma of the

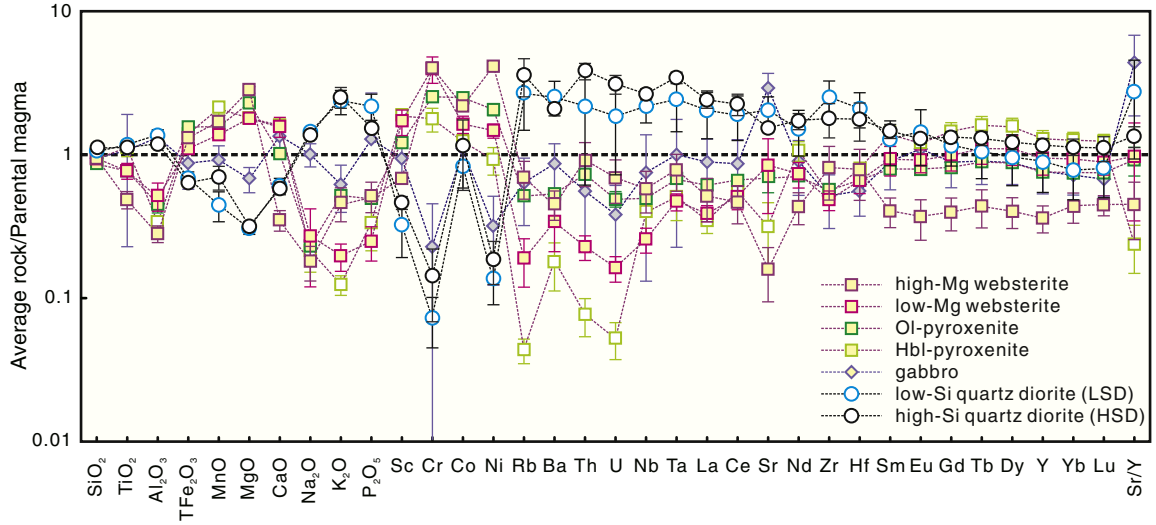

Fig. 10. Average compositions of the Ningcheng complex normalized to a primitive basaltic andesite from the NCC. The nominal parental magma is the late Mesozoic Guiyunhua hydrous high-Mg andesite that was derived from the enriched subcontinental lithospheric mantle beneath the NCC (Table S4; Ma et al., 2016). The Guiyunhua magmas are considered as (near-) primary magmas that equilibrated with mantle peridotite and have chemical compositions similar to primitive arc-derived basaltic andesites worldwide (Table S4; Grove et al., 2012).

Ningcheng complex probably was basalt or basaltic andesite derived from partial melting of the enriched lithospheric mantle beneath the NCC. Indeed, enriched mantle-derived mafic igneous rocks with high Sr/Y and La/Yb were widespread during Meosozoic time in the eastern China (e.g. Xu et al., 2004; Yang et al., 2012). We therefore speculate that fractional crystallization processes as well as inheritance of chemical compositions from such mafic parental magmas could be responsible for some Mesozoic adakitic rocks in the eastern China.

6.5. Implications for petrogenesis of adakitic rocks and TTGs

Our proposed petrogenetic model for the Ningcheng high-Mg adakitic rocks is not new. A subset of adakitic intermediate-felsic igneous rocks, both subduction-related and collision-related, have been interpreted as the products of crystal fractionation from basaltic magmas in the mid- to lower crust (e.g. Castillo et al., 1999; Chiaradia, 2015; Lee et al., 2007; Lu et al., 2015; Macpherson et al., 2006; Rodríguez et al., 2007). It is generally accepted that most primary magmas in subduction zones are basaltic or basaltic-andesite in composition and are H_2O-rich (Grove et al., 2012). Hydrous mantle-derived magmas also have been identified in continental settings (Ma et al., 2012, 2016; Xu et al., 2004). Indeed, deep magma chambers are commonly found in compressional continental arcs (Chaussard and Amelung, 2012; Lee et al., 2014) and perhaps are present in continental setting (Ma et al., 2012, 2016). Crystal fractionation of these hydrous mafic magmas at mid- to lower-crustal pressures would develop high-

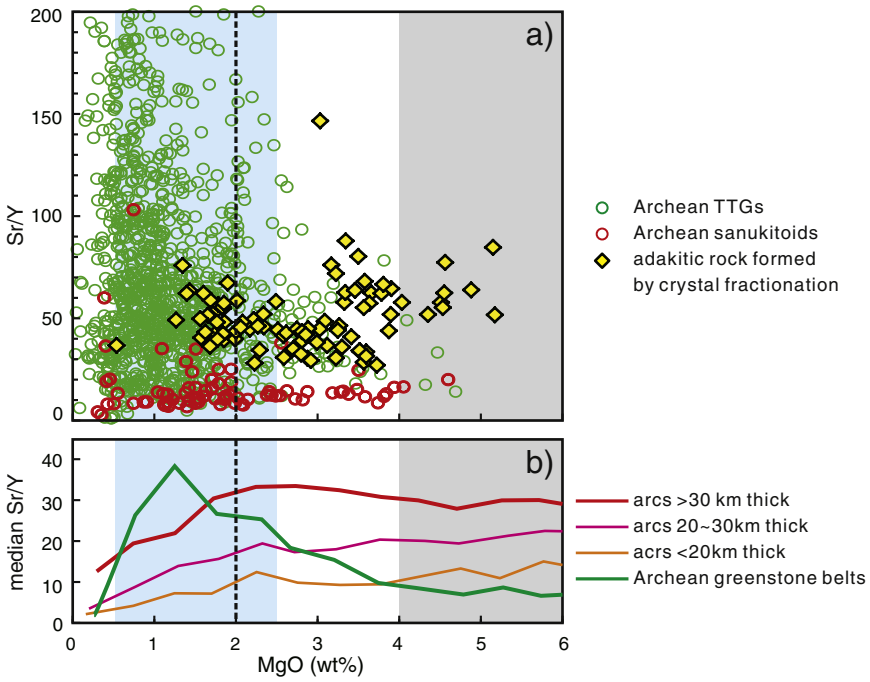

Fig. 11. (a) Plots of Sr/Y vs MgO for representative Phanerozoic adakitic rocks formed by fractionation of hydrous magmas and Archean granitoids (TTGs and sanukitoids). (b) Averages of median Sr/Y vs MgO for igneous rocks in modern arcs and Archean greenstone belt (Chiaradia, 2015). The gray and light blue areas represent Archean rocks with low median Sr/Y (<10) and high median Sr/Y (>20), respectively. Data for Phanerozoic differentiation adakitic rocks in (a) are from Castillo et al. (1999), Rooney et al. (2011), Li et al. (2013) and this study; data for Archean TTGs and sanukitoids in (a) are compiled from Moyen (2011) and Laurent et al. (2014), respectively.

Sr/Y adakitic signatures in the evolved magmas due to early fractionation of pyroxene, amphibole and perhaps garnet, and from suppression of plagioclase fractionation under high pH_2O conditions (Blatter et al., 2013; Müntener et al., 2001). The buffering effect of basaltic recharge or on-going underplating (Lee et al., 2014), if it occurred, could move the evolved magmas towards high-Mg adakitic rocks. However, arguments for these processes are based mainly on the geochemistry of high-Mg adakitic rocks, as complementary cumulate rocks are scarce. This study provides a rare example of an adakitic quartz diorite unit and an ultramafic-mafic unit in the Ningcheng complex as derivative magmas and complementary cumulates formed by the same process, by crystal fractionation of hydrous basaltic or basaltic andesitic magmas at mid- to lower-crustal pressures (e.g. Fig. 10).

The geochemical similarities between Phanerozoic adakitic rocks and Archean TTG suites have been recognized (Martin et al., 2005 for reviews), but there has been considerable debate on whether these two groups of igneous rocks formed by similar processes (Condie, 2005; Martin, 1999; Moyen and Martin, 2012; Smithies, 2000). Detailed discussions on their similarities and differences is beyond the scope of this paper; here we only assess the role of crystal fractionation of hydrous mafic magmas in the formation of the Phanerozoic and Archean high Sr/Y rocks by comparing relevant rocks in a Sr/Y vs MgO diagram (Fig. 11). Chiaradia (2015) showed that trends of median Sr/Y values versus MgO in modern arc magmas vary with arc thickness (Fig. 11b). The Sr/Y values of igneous rocks in thick (>30 km) arcs are high at intermediate MgO (2 ~ 6 wt%) and decrease when the magmas evolve to low MgO (<2 wt%); this trend can be reproduced by crystal fractionation of hydrous mafic magmas in the deep crust during the early differentiation stage (liquid with high MgO, H_2O and temperature). Moreover, representative adakitic rocks generated by crystal fractionation of hydrous mafic magmas show a trend of Sr/Y versus MgO (at intermediate MgO) resembling that of igneous rocks in thick arcs (Fig. 11a). Indeed, hydrous mantle-derived magmas and deep magma chambers are commonly found in compressional arcs (Chaussard and Amelung, 2012; Grove et al., 2012; Lee et al., 2014). An argument can thus be made in favor of an origin for some Phanerozoic adakitic rocks by crystal fractionation of hydrous mafic magmas in thick arcs. However, Archean rocks display different trends from their Phanerozoic "counterpart" in the Sr/Y vs MgO diagram (TTGs and sanukitoids shown in Fig. 11a; greenstone belt rocks shown in Fig. 11b); they are characterized by low Sr/Y at intermediate MgO and high Sr/Y at low MgO. These compositions indicate that other process (or processes), such as partial melting of basaltic rocks (Moyen and Martin, 2012) were mainly responsible for the origin of Archean low MgO, high Sr/Y granitoids (i.e. TTG suites). Therefore, crystal fractionation of hydrous mafic magmas is one of the efficient processes for making Phanerozoic high Sr/Y rocks but may not have been involved in the genesis of Archean granitoids. We further speculate that the Archaean TTG series is not an analogue of modern adakitic rocks and that the style of continental crust growth was different during Archean and Phanerozoic times.

7. Conclusions

Coexisting quartz diorites and websterite-pyroxenite-gabbros in the Ningcheng complex in the North China Craton are petrogenetically related, representing respectively fractionating melts and cumulates formed by crystal fractionation of hydrous mafic magmas at mid- to lower-crustal pressures. The quartz diorites acquired their adakitic signatures through a fractional crystallization process, rather than via high-pressure crustal melting. The Ningcheng complex thus presents one of the best cases for the crystal fractionation model for the genesis of adakitic rocks. Comparison with world-wide adakitic rocks suggests that differentiation of hydrous mafic magmas is an efficient process for producing Phanerozoic high Sr/Y rocks, but it was not important in the genesis of the Archean granitoids, for which other petrogenetic processes are needed.

Supplementary data to this article can be found online at http://dx.doi.org/10.1016/j.lithos.2016.05.024.

Acknowledgments

We thank Saokui Pan, Lubing Hong, Mingdao Sun. and Abing Lin for discussions and help in field work. This paper benefited greatly from significant and constructive comments from P. Castillo and an anonymous reviewer, as well as from the editorial handling by Sun-Lin Chung. This work was supported by the NSFC (41502040, 41130315, 9121404, 91014007; 70914001). This is contribution No. IS-2253 from GIG-CAS, 822 from the ARC Centre of Excellence for Core to Crust Fluid Systems, and 1087 from the GEMOC Key Centre.

References

Anderson, L.J., Smith, R.D., 1995. The effects of temperature and fO_2 on the Al-in-hornblende barometer. American Mineralogist 80, 549–559.
Atherton, M.P., Petford, N., 1993. Generation of sodium-rich magmas from newly underplated basaltic crust. Nature 362, 144–146.
Barnes, S.J., 1986. The effect of trapped liquid crystallization on cumulus mineral compositions in layered intrusions. Contributions to Mineralogy and Petrology 93, 524–531.
Blatter, D., Sisson, T., Hankins, W.B., 2013. Crystallization of oxidized, moderately hydrous arc basalt at mid- to lower-crustal pressures: implications for andesite genesis. Contributions to Mineralogy and Petrology 166, 861–886.
Carlson, R.W., Pearson, D.G., James, D.E., 2005. Physical, chemical, and chronological characteristics of continental mantle. Reviews of Geophysics 43 G1001.
Castillo, P.R., 2012. Adakite petrogenesis. Lithos 134-135, 304–316.
Castillo, P.R., Janney, P.E., Solidum, R.U., 1999. Petrology and geochemistry of Camiguin Island, southern Philippines: insights to the source of adakites and other lavas in a complex arc setting. Contributions to Mineralogy and Petrology 134, 33–51.
Chaussard, E., Amelung, F., 2012. Precursory inflation of shallow magma reservoirs at west Sunda volcanoes detected by InSAR. Geophysical Research Letters 39, L21311.
Chiaradia, M., 2015. Crustal thickness control on Sr/Y signatures of recent arc magmas: an Earth scale perspective. Scientific Reports 5, 8115.
Condie, K.C., 2005. TTGs and adakites: are they both slab melts? Lithos 80, 33–44.
Cooke, D.R., Hollings, P., Walshe, J.L., 2005. Giant Porphyry Deposits: Characteristics, Distribution, and Tectonic Controls. Economic Geology 100, 801–818.
Defant, M.J., Drummond, M.S., 1990. Derivation of some modern arc magmas by melting of young subducted lithosphere. Nature 347, 662–665.
Gaetani, G.A., Grove, T.L., Bryan, W.B., 1993. The influence of water on the petrogenesis of subduction related igneous rocks. Nature 365, 332–334.
Gao, S., Luo, T.C., Zhang, B.R., Zhang, H.F., Han, Y.W., Zhao, Z.D., Hu, Y.K., 1998. Chemical composition of the continental crust as revealed by studies in East China. Geochimica et Cosmochimica Acta 62, 1959–1975.
Gao, S., Rudnick, R.L., Yuan, H.L., Liu, X.M., Liu, Y.S., Xu, W.L., Ling, W.L., Ayers, J., Wang, X.C., Wang, Q.H., 2004. Recycling lower continental crust in the North China craton. Nature 432, 892–897.
Griffin, W.L., Andi, Z., O'Reilly, S.Y., Ryan, C.G., 1998. Phanerozoic evolution of the lithosphere beneath the Sino-Korean Craton. In: Flower, M.J., Chung, S.L., Lo, C.H., Lee, T.Y. (Eds.), Mantle Dynamics and Plate Interactions in East Asia. American Geophysical Union, Washington, pp. 107–126.
Grove, T., Parman, S., Bowring, S., Price, R., Baker, M., 2002. The role of an H_2O-rich fluid component in the generation of primitive basaltic andesites and andesites from the Mt. Shasta region, N California. Contributions to Mineralogy and Petrology 142, 375–396.
Grove, T.L., Till, C.B., Krawczynski, M.J., 2012. The role of H_2O in subduction zone magmatism. Annual Review of Earth and Planetary Sciences 40, 413–439.
Guo, F., Nakamuru, E., Fan, W., Kobayoshi, K., Li, C., 2007. Generation of palaeocene adakitic andesites by magma mixing; Yanji area, NE China. Journal of Petrology 48, 661–692.
Hammarstrom, J.M., Zen, E.A., 1986. Aluminum in hornblende: an empirical igneous geobarometer. American Mineralogist 71, 1297–1313.
Han, Q.J., Shao, J.A., Zhou, R., 2000. Petrology, geochemistry and petrogenesis of early Mesozoic diorites in Harqin area, Inner-Mongolia. Acta Petrologica Sinica 16, 385–391.
Hollister, L.S., Grissom, G.C., Peters, E.K., Stowell, H.H., Sisson, V.B., 1987. Confirmation of the empirical correlation of Al in hornblende with pressure of solidification of calc-alkaline plutons. American Mineralogist 72, 231–239.
Huang, F., Li, S., Dong, F., He, Y., Chen, F., 2008. High-Mg adakitic rocks in the Dabie orogen, central China: Implications for foundering mechanism of lower continental crust. Chemical Geology 255, 1–13.
Jagoutz, O., Müntener, O., Schmidt, M.W., Burg, J., 2011. The roles of flux- and decompression melting and their respective fractionation lines for continental crust formation: Evidence from the Kohistan arc. Earth and Planetary Science Letters 303, 25–36.
Jiang, N., Guo, J., Chang, G., 2013. Nature and evolution of the lower crust in the eastern North China craton: A review. Earth-Science Reviews 122, 1–9.
Laurent, O., Martin, H., Moyen, J.F., Doucelance, R., 2014. The diversity and evolution of late-Archean granitoids. Evidence for the onset of "modern-style" plate tectonics between 3.0 and 2.5 Ga. Lithos 205, 208–235.
Kay, R.W., 1978. Aleutian magnesian andesites: Melts from subducted Pacific Ocean crust. Journal of Volcanology and Geothermal Research 4, 117–132.

Leake, B.E., Woolley, A.R., Arps, C., Birch, W.D., Gilbert, M.C., Grice, J.D., Hawthorne, F.C., Kato, A., Kisch, H.J., Krivovichev, V.G., Linthout, K., Laird, J., Mandarino, J.A., Maresch, W.V., Nickel, E.H., Rock, N., Schumacher, J.C., Smith, D.C., Stephenson, N., Ungaretti, L., Whittaker, E., Guo, Y.Z., 1997. Nomenclature of amphiboles: Report of the subcommittee on amphiboles of the International Mineralogical Association, commission on new minerals and mineral names. American Mineralogist 82, 1019–1037.

Lee, C.T.A., 2014. Physics and chemistry of deep continental crust recycling. In: Holland, H.D., Turekian, K.K. (Eds.), Treatise on Geochemistry, Second edition Elsevier, pp. 423–456.

Lee, C.T.A., Morton, D.M., Kistler, R.W., Baird, A.K., 2007. Petrology and tectonics of Phanerozoic continent formation: From island arcs to accretion and continental arc magmatism. Earth and Planetary Science Letters 263, 370–387.

Lee, C.T.A., Lee, T.C., Wu, C., 2014. Modeling the compositional evolution of recharging, evacuating, and fractionating (REFC) magma chambers: Implications for differentiation of arc magmas. Geochimica et Cosmochimica Acta 143, 8–22.

Li, X., Liu, Y., Li, Q., Guo, C., Chamberlain, K.R., 2009. Precise determination of Phanerozoic zircon Pb/Pb age by multicollector SIMS without external standardization. Geochemistry, Geophysics, Geosystems 10, Q04010.

Li, X., Li, Z., Li, W., Wang, X., Gao, Y., 2013. Revisiting the "C-type adakites" of the Lower Yangtze River Belt, central eastern China: In-situ zircon Hf-O isotope and geochemical constraints. Chemical Geology 345, 1–15.

Liu, D.Y., Nutman, A.P., Compston, W., Wu, J.S., Shen, Q.H., 1992. Remnants of ≥3800 Ma crust in the Chinese part of the Sino-Korean craton. Geology 20, 339–342.

Liu, Y., Liu, H.C., Li, X.H., 1996. Simultaneous and precise determination of 40 trace elements in rock samples using ICP-MS. Geochimica 25, 552–558.

Liu, Y.S., Gao, S., Hu, Z.C., Gao, C.G., Zong, K.Q., Wang, D.B., 2010a. Continental and oceanic crust recycling-induced melt-peridotite interactions in the Trans-North China orogen: U–Pb dating, Hf isotopes and trace elements in zircons from mantle xenoliths. Journal of Petrology 51, 537–571.

Liu, S.A., Li, S., He, Y., Huang, F., 2010b. Geochemical contrasts between early Cretaceous ore-bearing and ore-barren high-Mg adakites in central-eastern China: Implications for petrogenesis and Cu–Au mineralization. Geochimica et Cosmochimica Acta 74, 7160–7178.

Lu, Y., Loucks, R.R., Fiorentini, M.L., Yang, Z., Hou, Z., 2015. Fluid flux melting generated postcollisional high Sr/Y copper ore-forming water-rich magmas in Tibet. Geology 43, 583–586.

Ludwig, K.R., 2003. User's manual for Isoplot 3.00: A geochronological toolkit for Microsoft Excel. Berkeley Geochronology Center Special Publication, Berkeley.

Ma, Q., Zheng, J.P., Griffin, W.L., Zhang, M., Tang, H.Y., Su, Y.P., Ping, X.Q., 2012. Triassic "adakitic" rocks in an extensional setting (North China): Melts from the cratonic lower crust. Lithos 149, 159–173.

Ma, Q., Zheng, J.P., Xu, Y.G., Griffin, W.L., Zhang, R.S., 2015. Are continental "adakites" derived from thickened or foundered lower crust? Earth and Planetary Science Letters 419, 125–133.

Ma, Q., Xu, Y.G., Zheng, J.P., Griffin, W.L., Hong, L.B., Ma, L., 2016. Coexisting early Cretaceous high-Mg andesites and adakitic rocks in the North China Craton: The role of water in intraplate magmatism and cratonic destruction. Journal of Petrology (accepted).

Macpherson, C.G., Dreher, S.T., Thirlwall, M.F., 2006. Adakites without slab melting: High pressure differentiation of island arc magma, Mindanao, the Philippines. Earth and Planetary Science Letters 243, 581–593.

Martin, H., 1999. Adakitic magmas: modern analogues of Archaean granitoids. Lithos 46, 411–429.

Martin, H., Smithies, R.H., Rapp, R., Moyen, J.F., Champion, D., 2005. An overview of adakite, tonalite-trondhjemite-granodiorite (TTG), and sanukitoid: relationships and some implications for crustal evolution. Lithos 79, 1–24.

McDonough, W.F., Sun, S.S., 1995. The composition of the Earth. Chemical Geology 120, 223–253.

Menzies, M.A., Fan, W.M., Zhang, M., 1993. Palaeozoic and Cenozoic lithoprobes and the loss of >120 km of Archaean lithosphere, Sino-Korean craton, China. Geological Society, London, Special Publications 76, 71–81.

Morimoto, N., Fabries, J., Ferguson, A.K., Ginzburg, I.V., Ross, M., Seifert, F.A., Zussman, J., Aoki, K., Gottardi, G., 1988. Nomenclature of pyroxenes. American Mineralogist 73, 1123–1133.

Moyen, J., 2009. High Sr/Y and La/Yb ratios: The meaning of the "adakitic signature". Lithos 112, 556–574.

Moyen, J., 2011. The composite Archaean grey gneisses: petrological significance, and evidence for a non-unique tectonic setting for Archaean crustal growth. Lithos 123, 21–36.

Moyen, J., Martin, H., 2012. Forty years of TTG research. Lithos 148, 312–336.

Müntener, O., Kelemen, P., Grove, T., 2001. The role of H_2O during crystallization of primitive arc magmas under uppermost mantle conditions and genesis of igneous pyroxenites: an experimental study. Contributions to Mineralogy and Petrology 141, 643–658.

Nandedkar, R., Ulmer, P., Müntener, O., 2014. Fractional crystallization of primitive, hydrous arc magmas: an experimental study at 0.7 GPa. Contributions to Mineralogy and Petrology 167, 1–27.

Pallares, C., Bellon, H., Benoit, M., Maury, R.C., Aguillón-Robles, A., Calmus, T., Cotton, J., 2008. Temporal geochemical evolution of Neogene volcanism in northern Baja California (27°-30° N): Insights on the origin of post-subduction magnesian andesites. Lithos 105, 162–180.

Putirka, K.D., 2008. Thermometers and barometers for volcanic systems. Reviews in Mineralogy and Geochemistry 69, 61–120.

Qian, Q., Hermann, J., 2013. Partial melting of lower crust at 10–15 kbar: constraints on adakite and TTG formation. Contributions to Mineralogy and Petrology 165, 1195–1224.

Richards, J.P., Kerrich, R., 2007. Special Paper: Adakite-like rocks: their diverse origins and questionable role in metallogenesis. Economic Geology 102, 537–576.

Ridolfi, F., Renzulli, A., Puerini, M., 2010. Stability and chemical equilibrium of amphibole in calc-alkaline magmas: an overview, new thermobarometric formulations and application to subduction-related volcanoes. Contributions to Mineralogy and Petrology 160, 45–66.

Rodríguez, C., Sellés, D., Dungan, M., Langmuir, C., Leeman, W., 2007. Adakitic dacites formed by intracrustal crystal fractionation of water-rich parent magmas at Nevado de Longaví Volcano (36·2°S; Andean Southern Volcanic Zone, central Chile). Journal of Petrology 48, 2033–2061.

Roeder, P.L., Emslie, R.F., 1970. Olivine-liquid equilibrium. Contributions to Mineralogy and Petrology 29, 275–289.

Rooney, T., Franceschi, P., Hall, C., 2011. Water-saturated magmas in the Panama Canal region: a precursor to adakite-like magma generation? Contributions to Mineralogy and Petrology 161, 373–388.

Schmidt, M.W., 1992. Amphibole composition in tonalite as a function of pressure: an experimental calibration of the Al-in-hornblende barometer. Contributions to Mineralogy and Petrology 110, 304–310.

Shao, J.A., Han, Q.J., Zhang, L.Q., Mu, B.L., 1999. Cumulate complex xenoliths in the early Mesozoic in eastern Inner Mongolia. Chinese Science Bulletin 44, 1272–1279.

Shao, J.A., Han, Q.J., Li, H.M., 2000. Discovery of the Early Mesozoic granulite xenoliths in North China Craton. Science in China Series D: Earth Sciences 43, 245–252.

Smithies, R.H., 2000. The Archaean tonalite-trondhjemite-granodiorite (TTG) series is not an analogue of Cenozoic adakite. Earth and Planetary Science Letters 182, 115–125.

Straub, S.M., LaGatta, A.B., Martin-Del Pozzo, A.L., Langmuir, C.H., 2008. Evidence from high-Ni olivines for a hybridized peridotite/pyroxenite source for orogenic andesites from the central Mexican Volcanic Belt. Geochemistry, Geophysics, Geosystems 9, Q03007.

Tu, X.L., Zhang, H., Deng, W.F., Ling, M.X., Liang, H.Y., Liu, Y., Sun, W.D., 2011. Application of resolution in-situ laser ablation ICP-MS in trace element analyses. Geochimica 40, 83–89.

Windley, B.F., Maruyama, S., Xiao, W.J., 2010. Delamination/thinning of sub-continental lithospheric mantle under eastern China: The role of water and multiple subduction. American Journal of Science 310, 1250–1293.

Xiao, W., Windley, B.F., Hao, J., Zhai, M., 2003. Accretion leading to collision and the Permian Solonker suture, Inner Mongolia, China: Termination of the central Asian orogenic belt. Tectonics 22, 1069.

Xu, Y.G., 2001. Thermo-tectonic destruction of the Archaean lithospheric keel beneath the Sino-Korean Craton in China: Evidence, timing and mechanism. Physics and Chemistry of the Earth Part A 26, 747–757.

Xu, Y.G., Huang, X.L., Ma, J.L., Wang, Y.B., Iizuka, Y., Xu, J.F., Wang, Q., Wu, X.Y., 2004. Crust–mantle interaction during the tectono-thermal reactivation of the North China Craton: constraints from SHRIMP zircon U–Pb chronology and geochemistry of Mesozoic plutons from western Shandong. Contributions to Mineralogy and Petrology 147, 750–767.

Yang, Y., Wu, F., Wilde, S.A., Liu, X., Zhang, Y., Xie, L., Yang, J., 2009. In situ perovskite Sr-Nd isotopic constraints on the petrogenesis of the Ordovician Mengyin kimberlites in the North China Craton. Chemical Geology 264, 24–42.

Yang, D., Xu, W., Pei, F., Yang, C., Wang, Q., 2012. Spatial extent of the influence of the deeply subducted South China Block on the southeastern North China Block: Constraints from Sr-Nd-Pb isotopes in Mesozoic mafic igneous rocks. Lithos 136-139, 246–260.

Zhang, H.F., Goldstein, S.L., Zhou, X.H., Sun, M., Zheng, J.P., Cai, Y., 2008. Evolution of subcontinental lithospheric mantle beneath eastern China: Re-Os isotopic evidence from mantle xenoliths in Paleozoic kimberlites and Mesozoic basalts. Contributions to Mineralogy and Petrology 155, 271–293.

Zhang, Z., Zhang, H., Shao, J.A., Ying, J., Yang, Y., Santosh, M., 2014. Mantle upwelling during Permian to Triassic in the northern margin of the North China Craton: Constraints from southern Inner Mongolia. Journal of Asian Earth Sciences 79, 112–129.

Zhao, G.C., Wilde, S.A., Cawood, P.A., Sun, M., 2001. Archean blocks and their boundaries in the North China Craton: lithological, geochemical, structural and P–T path constraints and tectonic evolution. Precambrian Research 107, 45–73.

Zheng, J.P., Lu, F.X., 1999. Mantle xenolith from kimberlites, Shandong and Liaoning: Paleozoic mantle character and heterogeneity. Acta Petrologica Sinica 15, 65–74.

Zheng, J.P., Griffin, W.L., O'Reilly, S.Y., Lu, F.X., Wang, C.Y., Zhang, M., 2004. 3.6 Ga lower crust in central China: New evidence on the assembly of the North China craton. Geology 32, 229–232.

Zheng, J.P., Griffin, W.L., O'Reilly, S.Y., Yu, C.M., Zhang, H.F., Pearson, N., Zhang, M., 2007. Mechanism and timing of lithospheric modification and replacement beneath the eastern North China Craton: Peridotitic xenoliths from the 100 Ma Fuxin basalts and a regional synthesis. Geochimica et Cosmochimica Acta 71, 5203–5225.

Zhu, R.X., Xu, Y.G., Zhu, G., Zhang, H.F., Xia, Q.K., Zheng, T.Y., 2012. Destruction of the North China Craton. Science China: Earth Sciences 55, 1565–1587.